# *Poleward expansion of tropical cyclone latitudes in warming climates*

Article

Accepted Version

# *POLEWARD EXPANSION OF TROPICAL CYCLONE LATITUDES IN WARMING CLIMATES*

***'In principle accepted' as a review article for Nature Geoscience***

Initial submission December 2020.

*Revisions prepared April, May, June 2021.*

*Further revisions prepared September, October 2021.*

Joshua Studholme*, *Yale University, CT, USA.*

Alexey Fedorov, *Yale University, CT, USA.*

Sergey Gulev, *Shirshov Institute of Oceanology, Moscow, Russia.*

Kerry Emanuel, *Massachusetts Institute of Technology, MA, USA.*

Kevin Hodges, *Reading University, Berks., UK.*

*Corresponding author email - joshua.studholme@yale.edu

**Abstract**

Tropical cyclones (TCs, aka hurricanes and typhoons) generally form at low latitudes with access to the warm waters of the tropical oceans but far enough off the equator to allow planetary rotation to cause aggregating convection to spin up into coherent vortices. Yet, current prognostic frameworks for TC latitudes make contradictory predictions for climate change. Simulations of past warm climates, such as the Eocene and Pliocene, show TCs forming and intensifying at higher latitudes than preindustrial conditions. Observations and model projections for the twenty-first century indicate TCs may again migrate poleward in response to anthropogenic greenhouse gas emissions, posing profound risks to the planet's most populous regions. Previous studies largely neglected the complex processes occurring at temporal and spatial scales of individual storms since these are poorly resolved in numerical models. Here we review this mesoscale physics in the context of the responses to climate warming of the Hadley circulation, jet streams and Intertropical Convergence Zone (ITCZ). We conclude that twenty-first century TCs will likely occupy a broader range of latitudes than over the last 3 million years as low latitude genesis will be supplemented with increasing midlatitude TC favourability, although precise estimates for future migration remain beyond current methodologies.

Tropical cyclones (TCs) start as $O(10^4)$ km$^2$ clusters of individual thunderstorms weakly rotating around a common axis. The transition into a TC involves increasing vorticity by two orders of magnitude to produce surface winds over 15 ms$^{-1}$[1.]; although it may take weeks for disaggregated convection to fully transform into a cyclone[2.]. Once formed, TCs generally move poleward and westward before interacting with midlatitude westerlies and weather systems, and in some cases transitioning into frontal systems (Fig. 1). Locally, the physics of evaporation, friction, convection, entrainment, and radiation determine the vortex lifecycle[3.][4.]. Box 1 summarizes these core elements in TC formation, intensification, and propagation – the TC lifecycle. How this local physics and the equator-to-pole TC distribution relate to one another has been discussed for at least a century[5.] and yet fundamental disagreement about how TC latitudes depend on climate persists[6.]. In this review we will synthesize recent advances and attempt to connect the heuristic view above with a well-defined physical basis for TC latitudinal distribution.

One of the central outcomes of this review is to establish the fundamental roles that convective mesoscale processes play in linking climatological TC occurrence to large-scale atmospheric dynamics in different climates. This emergent view is novel because the lifecycle evolution of TCs, and its intrinsic mesoscale processes, have historically been overlooked in TC climate studies. Instead, the focus has been on whether or not TCs would emerge from a given climatology of wind, temperature, and humidity[7.] (see section 'Tropical Cyclogenesis as a Dynamical Process'). This well-established framework is underpinned by empirical 'genesis potential indices' (GPIs) - best-guesses at the functional forms and coefficients for controls on TC formation that are calibrated against the observed TC distribution. Often GPIs are used in tandem with simple TC models either passively propagating cyclones through environmental winds (see Box 1) and neglecting their two-way interactions with the atmospheric environment (known as 'statistical downscaling')[8.].

These diagnostic methods are adopted in part because climate simulations with General Circulation Models (GCMs) struggle to resolve realistic TCs[9.]. A contrasting approach nests higher resolution models within lower resolution ones (known as 'dynamical downscaling'). Both dynamical and statistical downscaling approaches are used to enumerate how past, present, and future climates produce TCs (see section 'Past, Present, And Potential Latitudinal Migrations'). The problem is that these contrasting approaches yield vastly differing interpretations of twenty-first century climate projections[10.][11.][12.][13.] which thus establishes the necessity for prognostic understanding of the relationship between TCs and climate[6.]. In this review, we conclude that a joint consideration of the convective mesoscale processes occurring within TCs and the large-scale dynamics of the atmospheric Hadley circulation, Intertropical Convergence Zone (ITCZ) and tropospheric jet streams enables a new framework for understanding the relationship of TCs to climate (see section 'Linking Mesoscale Physics to Large-Scale Climate Dynamics'). As discussed later, these links have implications for reducing uncertainty in projections of twenty-first century TCs.

## TROPICAL CYCLOGENESIS AS A DYNAMICAL PROCESS

As a core methodology in modern TC-climate studies, GPIs reproduce the broad-brush characteristics of observed TC genesis, particularly at the basin averaged scale[3.]. GPIs do significantly worse at reproducing characteristics of TC genesis simulated in GCM simulations[9.][14.]. We note that while appropriate GPI formulations should only use variables explicitly relevant to TC physics, they often use free tropospheric relative humidity rather than water vapor saturation deficit (or free tropospheric dryness relative to the boundary layer) as the moisture variable despite the established physical relevance of the latter but not the former[15.]. While GPI variants perform equally well in reproducing TC genesis patterns of current climate, they diverge in describing future changes[15.]. Moreover, the greenhouse

warming response of an individual state-of-the-art GPI, that used the physically consistent moisture variable of saturation deficit, was shown to change sign when the empirical coefficient for that variable was modified without degrading the fit to observations[11.]. More troubling still, the statistical relationship between the time-mean environmental fields used to calculate GPIs and TC distribution is not necessarily consistent between the observations and models, and between models using different dynamical cores, resolutions, and physics[16.][17.].

Behind GPIs is the assumption that climatological tropical cyclogenesis, approximated as genesis potential, is a localised process. This assumption therefore abstracts away the complex set of planetary, synoptic, and mesoscale processes that give rise to the observational distributions against which GPIs are calibrated. The problem is that these processes resulting in cyclogenesis and intensification occur over a wide range of overlapping spatial and temporal scales and can be dislocated from one another[16.][18.][19.][20.] (see Extended Data Figs. 1 and 2 for examples). This issue likely gives rise to the aforementioned apparent limitations of GPIs. Thus, to generate fundamental understanding of physical controls over TC distribution with robust prognostic skill requires making explicit the links between the synoptic and mesoscale processes inherent to TCs and the large-scale dynamics within which they emerge, intensify, and dissipate.

It is remarkable that the relationship between convective mesoscale processes underpinning TCs and large-scale dynamical structures has been largely ignored[21.][22.] since the first GPI was published in 1979[7.]. This is all the more striking because much observed TC genesis is embedded within the belts of climatological convection that are very well studied: roughly 70% of first recorded TC positions occur within the ITCZ (inside the green contour in Fig. 2a). Idealised simulations, historical evidence, and paleo-climatological reconstructions[23.][24.][25.] all find strong relationships between ITCZ characteristics and TC frequency.

Diversity in TC genesis mechanisms (Fig. 1) is part of this problem and presents a challenge for deriving a simple prognostic framework for TC genesis and intensification. While typically TC genesis occurs in non-baroclinic large-scale environments, 30% of genesis events do involve baroclinic influence[26.]. Globally, one in six TCs form via 'tropical transition' whereby transient upper tropospheric disturbances trigger deep convection and low-level moisture convergence upon coinciding with lower tropospheric lows[27.] (Fig. 1b and Extended Data Fig. 2). This process is possible over much lower sea surface temperatures (SSTs, < 17°C) and at higher latitudes (>40 °N) than canonical TC genesis[28.]. These upper tropospheric disturbances originate from anticyclonic wave breaking following planetary wave amplification and thus have strong, established sensitivity to planetary warming[29.]. GPIs computed at higher frequency can capture some of these 'non-traditional' genesis pathways, including polar lows and Mediterranean hurricanes[30.] (Extended Data Fig. 3), but these routes are poorly captured by GPIs computed from monthly mean variables as is done nearly universally. Significantly, genesis pathways that are marginal in the present day may have been non-marginal in the past and may become non-marginal again as climate warms[31.][32.][33.][34.].

Most non-canonical genesis pathways occur on the poleward edge of the TC distribution. On the equatorward side, convectively coupled equatorial waves (CCEWs), easterly waves (EW) and the Madden-Julian Oscillation (MJO) play a critical role in TC genesis and intensification[4.], which further complicates analysis of climates' TC favourability. These synoptic and mesoscale convective phenomena can all trigger convective aggregation but also interact with each other [35.]. CCEWs are estimated to be involved in ~85% of North Atlantic and western North Pacific TC genesis events[36.][37.], enabling the necessary convective organisation for genesis[38.]. However, this may simply determine the location and timing of genesis, not overall TC frequency[39.]. Indirectly, CCEWs can

condition the atmosphere to either encourage or suppress TC genesis locally as their convective anomalies modulate vorticity, temperature, moisture, and wind shear at a range of scales. They also induce remote responses[40.][41.][42.] such as far-field suppression of TC potential intensity (PI; see Box 1) via upper tropospheric temperature homogenisation maintaining weak horizontal temperature gradients in the tropics (the WTG; see Box 1).

## PAST, PRESENT, AND POTENTIAL LATITUDINAL MIGRATIONS

### *(a.) Paleoclimate reconstructions and modelling*

At geologic timescales, it is likely that the secular cooling throughout the Cenozoic (the past 66 million years) resulted in the contraction of latitudes with both high genesis potential and PI towards the equator in both hemispheres (Fig. 3)[43.]. This would have been coincident with contraction of the Hadley circulation and equatorward shifts in the subtropical jet streams[43.]. During the Early Eocene climate optimum (53-51 million years ago) – the warmest prolonged climate interval of the Cenozoic – paleo-proxies show atmospheric $CO_2$ concentrations around 1400 ppm (with a very large uncertainty range[44.]). This may have resulted in the equator-to-pole temperature gradient being up to 10 °C flatter than the modern era[45.][46.] and summertime surface continental temperatures in the Arctic reaching ~23 °C[47.]. During the geologically brief Paleocene-Eocene Thermal Maximum (PETM, ~55 mya), these differences were likely even more exaggerated[48.][49.].

While the circulation dynamics associated with Eocene climate remain under debate[45.][50.], available reconstructions and climate models forced with Eocene continental configuration and $CO_2$ concentrations suggest increased extratropical humidity, poleward jet stream shifts, and Hadley circulation expansion relative to present[43.][47.][51.][52.][53.]. This implies a marked poleward expansion of areas favourable to TC formation and intensification (Fig. 3; Extended Data Fig. 4). Eocene simulations show genesis potential centred around the

subtropics (~25 degrees latitude) in both hemispheres in contrast to the modern era where it dominates the deep tropics (~10 degrees latitude)[34.][43.](Fig. 3c). Moreover, a recent PETM simulation using a 25 km horizontal resolution atmospheric GCM shows very strong suppression of low latitude TCs, and both hemispheres' midlatitudes (30-60 degrees latitude) producing many TCs[34.] (Figure 3b). These results agree with cloud-system resolving simulations of an idealized Eocene-like climate[32.] (Fig. 5, yellow line).

Contemporary TC distributions were likely established sometime towards the end of the warm Pliocene[43.][54.] (2.6-5.3 million years ago). For most of this period, proxy-based reconstructions indicate atmospheric $CO_2$ concentrations 350-450 ppm[55.], latitudinal SST gradients up to 5°C degrees flatter than present[56.], and surface westerlies weaker and possibly more poleward[57.]. In addition, Pliocene climate may have featured an expanded low-latitude warm pool, reduced equatorial and coastal upwelling, weakened Hadley circulation, and TC activity enhanced and shifted poleward relative to present[54.][58.][59.][60.]. During the late Pliocene, atmospheric $CO_2$ decline among other factors led to the establishment of colder climate patterns culminating with the onset of northern hemisphere glaciation[61.]. This marked the start of a period, ending in the present century, when latitudinal variations in TCs became more muted and were primarily controlled by orbitally driven insolation changes and resultant glacial cycles, shorter millennial climate variability, and varying aerosol emissions.

GCMs forced with continental ice sheet reconstructions and low atmospheric $CO_2$ concentrations (185 ppm) indicate that the planet's TC distribution during the Last Glacial Maximum (LGM, 21 k.y.a) was not significantly different from the present day albeit mean TC intensity was likely lower[62.][63.][64.]. These models however disagree over large-scale atmospheric circulation structure, specifically over whether the southern hemisphere subtropical jet was poleward or equatorward relative to modern and whether atmospheric

convection in western Pacific was stronger or weaker[65.][66.]. Since the LGM, multi-millennial scale TC variability was likely dominated by the slow increase in the boreal summer equator-to-pole insolation gradient until ~10 kya and the subsequent decline associated with orbital precession[67.]. The increased insolation gradient at the precession minima (~10 kya) may have caused amplified tropical convection and strengthened midlatitude jets[68.][69.][70.][71.]. This seems to correspond to suppressed genesis potential of the most equatorward TCs[67.].

Orbitally driven variations were punctuated by millennial-scale abrupt climate changes, including the cold Heinrich and the Younger Dryas events. The slowdown of Atlantic Meridional Overturning Circulation[72.] (AMOC) typically associated with those events cooled the North Atlantic, suppressing PI[67.]. The increased meridional temperature gradient in the northern hemisphere would have led to an intensification and equatorward shift of both the subtropical jet and Hadley cell[73.][74.], presumably suppressing higher latitude TC genesis and intensification[67.]. Changes in large-scale climate over the last 21 thousand years ($CO_2$ ~180-280 ppm) were likely smaller in comparison to changes driven by atmospheric $CO_2$ since the Eocene ($CO_2$ ~500-2000 ppm) and Pliocene ($CO_2$ ~300-500ppm): in particular, mean ITCZ shifts since the LGM were probably less than 1 degree latitude[75.].

Atmospheric aerosols provide an additional control on shorter timescales. They were suppressed during the "green Sahara" period centred around the mid-Holocene[76.][77.] (6 k.y.a.) but sporadically increased following volcanic eruptions[25.][78.]. Mineral dust has hemispherically asymmetric impacts on temperature, and consequentially ITCZ location[79.] and tropical cyclone latitudes[25.]. Further north, reduced dust increases SSTs, which results in PI increases and poleward jet shifts expanding regions of tropical cyclone favourability[25.][76.][77.]. Moreover, North Atlantic TCs were probably shifted poleward relative to present as Sahara greening caused a poleward displacement of easterly waves[76.][77.].

Over the last two thousand years, model simulation based GPI and PI show no secular trends prior to the Industrial Revolution[78.][80.]. Integrated Atlantic paleo-tempestological records (16 – 32 °N) however suggest persistent poleward migration of eastern tropical Atlantic TCs over the last 450 years in concert with ITCZ poleward migration[81.]. Other records show TC activity shifting from the Caribbean and Gulf of Mexico toward the Bahamas and New England around A.D 1400, correlated with warm central tropical Atlantic SSTs prior to this shift and a relatively warmer western North Atlantic afterwards[82.]. This would have been coincident with high basin-integrated TC activity in the Medieval Warm Period (MWP; A.D. ~900 – 1450) followed by a lull during the Little Ice Age[83.] (LIA; A.D. ~1450 – 1850). Paleo-reconstructions and historical evidence imply poleward western North Pacific TC and ITCZ shifts during the MWP and equatorward shifts during the LIA[24.][84.]. The North Atlantic poleward and western North Pacific equatorward TC shifts across the MWP-LIA transition occurred, presumably, with Pacific warm pool cooling, Pacific Walker circulation weakening, East Asian summer monsoon weakening and a narrowing and southward shift in the ITCZ[84.][85.]. Finally, tree rings suggest a secular twentieth century TC poleward migration in the western North Pacific (33-45 °N)[86.].

TC activity may also fluctuate with changes in ENSO, Atlantic Multidecadal Variability (AMV) and the Pacific Decadal Oscillation (PDO) over centennial and millennial timescales[83.][87.]. The MWP-LIA transition arguably marked an increase in ENSO amplitude, a change from predominately negative to predominately positive AMV, and change from a persistent negative PDO state to a muted PDO signal (ref. [88.] reviews these modes throughout the Holocene). Most casual interpretations of TC latitudinal variability in the paleo-records over centennial to millennial timescales are understood via connections to the ITCZ, often mediated by ENSO variability[24.][81.][89.]. Further, TC coupling to large-scale stationary circulation features like the subtropical highs is also recognised[25.][81.][90.].

We stress that reconstructions of TCs throughout Earth's history suffer large uncertainties. Model biases and uncertainties in boundary conditions and radiative forcing diminish the utility of climate simulations and their GPI estimates. There is even continued debate over how TCs are identified and tracked in these numerical simulations[13.]. Conversely, proxy-based TC reconstructions only record local storm transits and are biased towards intense events near coastlines[91.], while centennial variability in individual paleorecords of intense TCs may be random and not reflective of large-scale climate dynamics[92.]. Thus, synthesising paleo-hurricanes records is important, yet complicated by significant spatial under-sampling[93.].

*(b.) Poleward TC migration in recent observations*

Subtle but robust poleward trends of 53 ±43 and 62 ±48 km per decade[94.] in TC seasonal-mean LMI latitudes are detectable in observations of the northern and southern hemispheres respectively (1982 to 2012). While these estimates are largely drawn from analyses of the IBTrACS archive, which aggregates multiple records, such poleward migration is found across different datasets and also for genesis latitudes[94.][95.][96.]. The magnitudes of these trends depend on the period and TC intensity considered[94.]. Life-time maximum intensity is used since it does not rely on absolute intensity magnitudes which are inconsistently recorded and poorly represented in reanalysis[94.][97.]. Dynamical reanalysis data reproduce TC LMI latitudes mostly within a few degrees of observations[97.]. However, simulated TCs tend to persist too long into high latitudes where they expand radially and become better resolved thus achieving higher intensities there and distorting higher latitude (>30 °) LMI estimates[97.]. Thus, satellite-based records provide the most reliable source for trends in TC latitudes.

Over half the recently observed poleward migration is explained by inter-basin frequency changes (Fig. 2d), with the North Atlantic (average LMI 2,800 km from the equator versus hemispheric mean of 2,150 km) and South Pacific (1,990 km vs 1,900 km) increasingly producing more cyclones relative to other basins in the same hemisphere[94.][98.]. Poleward migration is also not uniform over LMI latitude percentiles[96.] and one of the most equatorward hurricanes on record occurred in 2016 (Hurricane Pali, ~2.3ºN). These present-day trends appear to be associated with changes in both the ocean (SST patterns; Fig. 4a), and atmospheric thermodynamics (PI; Fig. 4b), and dynamics (vertical shear, large-scale tropospheric winds)[94.][96.][99.]. Additionally, genesis potential has increased during this period (Fig. 4e). Twentieth-century global-mean SST increases may have forced increases in storm radii in the western North Pacific TCs[100.]. These larger TCs tend to propagate further poleward following increased beta drift (Box 1) and interaction with the subtropical highs and tropical upper tropospheric troughs (TUTTs)[101.]. These poleward migration trends are coincident with increase rates of observed extratropical transition[102.].

In addition to observed gradual poleward migration, pronounced transient zonal and meridional TC migrations occur in response to ENSO, PDO and AMV cycles[103.]. During negative PDO phases (warmer SSTs in the western and central subtropical Pacific), maximum PI latitudes extend poleward, encouraging higher latitude Pacific TC genesis[104.]. Poleward migration of North Atlantic TCs associated with ENSO occurs following both dynamic and thermodynamic suppression of low latitude TCs. During El Niño, Pacific Walker circulation weakening intensifies upper-tropospheric westerlies over the North Atlantic amplifying vertical wind shear over the Caribbean and eastern Northern Pacific[105.][106.], while CCEWs originating in the Pacific push the tropical North Atlantic atmosphere out of thermodynamic equilibrium with its underlying SSTs to suppress TC genesis[41.].

Over the past three to four decades the west-east equatorial SST gradient across the tropical Pacific has strengthened, with the eastern equatorial Pacific getting colder while the western Pacific warmer, and the Walker circulation intensified[107.][108.][109.]. This trend pattern may reflect a negative PDO phase with possible contributions from aerosol effects and a thermostat-like response to greenhouse gas forcing[109.]. Transition to a positive AMV circa A.D. 2000 [108.][110.] and greater inter-basin temperature contrasts[107.] are also invoked to explain this strengthening of the Walker circulation. Regardless of the cause, the stronger Pacific Walker circulation has intensified vertical wind shear over the equatorial central Pacific and the deep tropical North Atlantic, contributing to TC poleward migration[98.][110.].

In contrast, by century's end, a relaxation of the SST gradient across the Pacific with pronounced eastern equatorial Pacific warming and corresponding weakening of the Walker circulation are projected in nearly all CMIP6 models[109.]. All else being equal, this would correspond to lower vertical wind shear over the equatorial central Pacific and equatorial North Atlantic, an equatorward ITCZ shift and thus encouraged low latitude TC formation and intensification.

*(c.) Simulated climate change*

Idealised aquaplanet TC simulations (no continents, see ref.[23.] for a review) have been conducted with atmospheric models and fixed SSTs or simplified 'slab-ocean' representation of fixed oceanic heat transport (via the '*q*-flux' abstraction). These simulations generally neglect zonal climate asymmetries and the seasonal cycle and have other limitations. For example, only models with dynamic oceanic heat transport can provide strong negative feedback on ITCZ displacements. Consequentially, changes in ITCZ position and strength under variable climatic forcing differ dramatically between aquaplanet and fully-coupled simulations – in the former the ITCZ can move poleward by 10-20 degrees latitude,

315 while in the latter ITCZ intensity changes but its shifts do not exceed ~1 degree[111.]. In
316 addition, aquaplanet ITCZs are sensitive to model resolution and convective
317 parameterisation[112.].

318 Nevertheless, aquaplanet simulations with imposed atmospheric cross-equatorial heat
319 transport variations suggest a TC genesis scaling of a 40 % increase in global TC frequency
320 per degree of latitude of poleward ITCZ shift[113.]. However, increases in TC genesis can
321 occur on warming aquaplanets even with an equatorward ITCZ shift as changes in the
322 subtropical jet and reductions in midlatitude baroclinicity increase the likelihood of TC
323 genesis (Fig. 5). Aquaplanet TC activity appears to be correlated with atmospheric static
324 stability but is only sensitive to vertical shear above a certain threshold value (~5 m $s^{-1}$; [114.]).
325 The climatological relationship of TC latitudes with PI seems to be weak and non-
326 monotonic[31.][32.][114.]. Rather, poleward migrations reflect the aerial expansion of high (>70
327 m $s^{-1}$) PI values. These poleward migrations follow tropical expansion, but not simply the
328 concurrent dilation of the Hadley circulation[33.].

329 Full continent slab-ocean, statistical downscaling experiments with large $CO_2$
330 increases (x8 and x32 preindustrial concentration) show LMI poleward migration (1.6°, 7.4°
331 respectively) and prolonged TC lifecycles[31.]. Overall maximum PI does not increase with
332 these hyper-exaggerated warmings (consistent with ref. [114.]). This statistical downscaling
333 method involves inserting $O(10^6)$ artificial random weak vorticity anomalies (referred to as
334 TC 'seeds') over the global ocean in an effort to simulate realistic pre-TC disturbances which
335 – as we stress above - may come from a number of spatially and temporally variable
336 processes, potentially poorly resolved in GCMs (Fig. 1 and Box 1). Most of these artificial
337 vorticity anomalies decay rapidly, but a few survive and are then passively advected by the
338 large-scale winds and beta drift. Computing the thermodynamics of these vortices yields the
339 corresponding TC lifecycle (i.e. the progression through genesis, intensification and

cyclolysis; this methodology does not represent extratropical transition). The results from this approach depend on the number of "seeds" used and thus this method requires calibration to reproduce realistic TC frequency[115.].

Some coupled 2x and 4x $CO_2$ experiments with dynamically simulated TCs exhibit small poleward shifts of several degrees of latitude in the northern hemisphere[116.], but other coupled 2x$CO_2$ experiments find zonal, but not poleward TC migration[16.]. Ref. [16.] find that in these experiments the pre-TC synoptic and convective mesoscale disturbances, defined as seasonal variance in 3-10 day bandpassed 850 hPa vorticity, are the principle atmospheric driver of TC frequency responses in increasing $CO_2$ simulations. Such TC source disturbances are found to be highly concentrated within climatological convection (the ITCZ and Pacific Warm Pool) with potential links between their frequency and time-mean local tropospheric pressure velocity, $\bar{\omega}$ [1.]. This result contrasts with statistical downscaling methods that assume a constant number of TC "seeds" (the artificially inserted pre-TC source disturbances), but does not invalidate the random seeding approach as long as the "seeds" are sufficiently weak and numerous.

Attribution work using coupled models finds that recent TC distribution changes are very likely anthropogenically forced[117.]. However, CMIP5 models and various regional downscaling experiments project a range of 21st century TC migration scenarios from no further migration, to poleward LMI migration of a few degrees (but less than the 5 degrees implied by continuation of the ½ degree per decade trend[94.]), and zonal migration of Pacific TCs[118.][119.]. Early analysis of CMIP6 finds no consensus on 21st century distribution changes in explicitly resolved TCs[13.] but statistical downscaling shows poleward migration in the northern hemisphere, particularly in the North Atlantic[11.]. Climate models' dynamically resolved TC activity is projected to be globally suppressed by greenhouse gases; however, statistical downscaling predicts increases in line with monthly-mean GPI values

365 that reflect increasing PI and decreasing wind shear tempered against increasing mid-
366 tropospheric relative dryness[11.][12.][120.].

367 Some broad patterns in end-of-century TC predictions have been established, although
368 the statistical reliability of these findings depends upon the selection of climate models
369 studied. In the northern hemisphere, TC poleward shifts of a few degrees in the North
370 Atlantic and both sides of the North Pacific alongside the suppression of the most western of
371 Pacific TCs is found in some but not all analyses[102.][121.][122.]. This is accompanied by a shift
372 in Pacific TC activity towards the central Pacific[123.] and increasing recurvature of western
373 North Pacific TC tracks[118.][124.]. Southern hemisphere projections show no clear deviation in
374 TC genesis latitudes between current and future climate[11.][119.]. However, statistical
375 downscaling of CMIP6 models shows a significant poleward expansion of TC activity both in
376 the North Atlantic and South Indian oceans[11.]. All these projections of increased high
377 latitude TC activity under greenhouse warming are consistent with other projections of
378 increased rates and intensity of extratropical transition in the western North Pacific and North
379 Atlantic[125.][126.][127.]. Additionally, TC translation speed is projected to decrease over the 21st
380 century, following poleward shifts in the midlatitude westerlies, which would increase
381 midlatitude TC track density[128.].

382 While GCMs do reproduce modern TC *climatologies* reasonably well, strong errors
383 persist particularly at the distribution edges[117.][118.][119.]. Models overestimate historical
384 genesis rates in the central North Pacific and the southern hemisphere but underestimate
385 eastern North Pacific and North Atlantic TCs[11.][13.][129.] . Although SST patterns are
386 considered the principal cause behind spreads in projected TC climatologies[12.][16.], this
387 implicates a complex set of processes such as AMOC slowdown and radiative feedbacks.
388 Moreover, inter-model spread in projected SSTs cannot account entirely for the lack of

consensus and another likely factor is differences in models' representation of atmospheric deep convection[129.][130.].

## LINKING MESOSCALE PHYSICS TO LARGE-SCALE CLIMATE DYNAMICS

An emergent hypothesis explaining recent TC poleward migration relates it to observed tropical expansion through the areal expansion of low vertical wind shear and high PI regions of the subtropics[94.]. This invokes changes in the latitudes of the descending branches of the Hadley circulation and midlatitude jet streams. PI has increased in recent decades (Fig. 4b) and model simulations indicate that changes in TC distribution track the aerial expansion of high PI values[78.][114.]. Such an expansion, which follows increasing modified Carnot efficiency and lower TC outflow temperatures (Box 1), is present in the recent record (Fig. 4d,f). These results broadly agree with the Eocene and Pliocene model reconstructions showing wider tropics during those epochs coincident with higher latitude TC activity. However, assumptions of tropical expansion *causally driving* TC poleward migration require careful examination[33.]. As the limitations of GPIs and existing frameworks have shown, the challenge lies in integrating the sensitivity of convective mesoscale processes to planetary temperature with the summertime mean circulation's broader sensitivities, including the jet stream shifts, Hadley cell expansion and ITCZ changes[131.][132.][133.], each driven by their own distinct set of dynamics.

One major confounding aspect of process-based understanding of recent subtropical decrease in vertical wind shear and increase in PI[94.] is the link – or lack thereof – between changes in the Hadley cells and the subtropical jet. A ~1/2° per decade poleward expansion of the Hadley cells, normally shorthand for 'the tropics', can be identified in several metrics and datasets[132.]. However, no robust trend is found for the subtropical jet[134.], despite the expectation that they would covary because the subtropical jet enables strong vertical wind

shear and the Hadley cell terminates where the shear is maximal[135.]. The much weaker poleward trend, if any, in the subtropical jet implies that different aspects of tropical expansion are only partially coupled[136.].

The latitude of the Hadley cell edge is however negatively correlated on interannual timescales, at least in CMIP5 models, with the *strength* (not latitude) of the subtropical jet[137.]. Furthermore, the coherent midlatitude jet stream in the time-mean zonal-mean circulation represents the superposition of two distinct, yet dynamically connected features: the subtropical jet and the eddy-driven jet at higher latitudes. The Hadley cell edge is shown to be positively correlated with the latitude of the eddy-driven jet[138.], but not of the subtropical jet. While midlatitude baroclinicity associated with the eddy-driven jet is relatively weak during TC seasons, it still produces significant wind shear[139.]. How this relationship between the Hadley cell edge, eddy-driven jet latitude and subtropical jet strength affects the synoptic and mesoscale processes of baroclinically enabled TC genesis[26.], intensification and extratropical transition (Fig. 1b) remains a pressing open research question. Indeed, this type of TC genesis becomes common in the midlatitudes in idealised models of warm climates[31.][32.][33.][34.], in particular when the two jets split (Fig. 5; Extended Data Fig. 5). In these simulations the summer subtropical jet shifts equatorward while the eddy-driven jet shifts poleward.

A separate explanation for recent TC poleward migration invokes suppressed genesis in the deep tropics caused by increased dry static stability in the warming tropical atmosphere[99.] (Fig. 4a). However, the extent to which changes in time-mean static stability effect actual TC processes is unclear. We suggest that static stability is best viewed as a co-factor with PI since both are related to atmospheric lapse rates. In fact, concurrent observations exhibit long-term increases in higher-frequency CCEWs[140.] and increases in ITCZ precipitation (Extended Data Fig. 6), which contradicts the assertion that increased

time-mean static stability implies less convective activity. Besides, SST increase in the deep tropics also leads to both greater mid-tropospheric 'saturation deficit' (or tropospheric dryness relative to the boundary layer), a well-established thermodynamic TC inhibitor[115.][141.], and potentially also poleward shifts in the midlatitude westerlies[133.], which would likely correspond to aerial expansion of favourable TC latitudes with high PI and lower vertical shear.

Another core aspect in discussions of TCs and climate change is ITCZ migrations and dynamics, even though ITCZ responses to warming may depend on the metric considered and have been muted during recent climate change[131.]. Despite large inter-model differences, overall precipitation responses in CMIP6 models show a stronger, wider, and equatorward ITCZ by the end of the twenty-first century (Fig. 6, Extended Data Fig. 7), which follows changes in SST patterns and constraints from the Clausius-Clapeyron relation (the "wet gets wetter" paradigm[142.]). However, unlike the precipitation-based metrics used here, circulation measures computed for in the previous CMIP5 models showed only little ITCZ latitudinal changes, with muted narrowing and weakening[131.]. Reconciling these differences will be critical to understanding changes in low latitude TCs in the 21$^{st}$ century.

Idealised simulations confirm that the further off-equator the ITCZ is, the more ambient vorticity is available for TC genesis[1.][143.]. The wider and stronger it is by precipitation measures, the higher free tropospheric specific humidity is likely to be[23.]. Lastly, experiments with the moist shallow water equations indicate that a more poleward ITCZ is more susceptible to barotropic instability[144.]. All these factors would enhance TC genesis, but how these idealized inferences of TC dynamics relate to more realistic ITCZs, and GCM biases, is not yet fully examined.

Changes at both the tropical-extratropical margin and within the ITCZ also raise questions about the degree of independence between source disturbances for TCs and the

mature cyclones themselves. For example, suppressing easterly waves in the North Atlantic, the primary source of pre-TC disturbances there, may alter the location and timing of genesis, but not overall TC frequency[39.]. Moreover, the stronger the ITCZ is by circulation measures, the more initial disturbances may be available for TC genesis[1.][16.]. However, the ITCZ is strong and well defined in the central North Pacific where TC genesis is sparse (Fig. 2a), confirming that the climatologies of source disturbances and TC development can be dislocated.

Indeed, convective organisation is possible through multiple pathways such as CCEWs, MJO, easterly waves, barotropic ITCZ breakdown, convective self-aggregation and, in the Indian Ocean, orographically induced vortices[2.][32.][145.][146.][147.] (Fig. 1b). Yet, investigating the resultant pre-TC disturbances with contemporary climate GCMs is problematic since models struggle to propagate convective disturbances realistically because of their mismatch between surface wind convergence and precipitation patterns caused by convective parameterisations[148.]. As the realism of model simulations improves, it will become possible to ask: *What is the best way to identify these pre-TC convective disturbances? How strongly are these disturbances linked to CCEWs? What are the climate sensitivities of these waves and disturbances? How are they affected by changes in ITCZ latitude, width, and strength?*

While the previous paragraphs discussed the potential links between convective mesoscale processes and large-scale circulations, changes in the thermodynamic contribution to TC genesis and intensification favourability are also critical. These are likely tied to SST changes with greenhouse warming as PI increases in a pattern not dissimilar to tropical SST changes (compare Fig. 4 a and b), which may be related to recent time-mean enthalpy flux increase (Extended Data Fig. 8) concomitant with SST warming (Fig. 4a)[110.]. At the same time, since most atmospheric moisture is in the lower troposphere and its content grows exponentially following the Clausius-Clapeyron scaling, the lower levels gain more water

vapor with warming than the free troposphere. The resultant increase in the relative dryness of the free troposphere (with respect to the boundary layer) discourages genesis[115.]. This effect could be the strongest thermodynamic control over TC formation in a warming climate[11.], but since moisture in the free troposphere is not controlled by the WTG, it can vary across longitudes and depend on the large-scale tropical circulation (Box 1).

This entire discussion has been focused on how the synoptic and mesoscale processes critical to the TC lifecycle respond to climate change as manifested in the time-averaged planetary-scale fields. We have neglected consideration of feedbacks of TCs upon climate itself. Three particular effects are noteworthy: the effect of TCs in drying free troposphere[3.], TCs' role in the upper ocean mixing and oceanic heat transport[3.][54.][149.][150.], and low-cloud suppression by TCs[151.]. These effects are not well-handled by GCMs and may significantly affect their responses to radiative forcing, especially in paleo-context[54.][150.].

## IMPLICATIONS FOR TWENTY-FIRST CENTURY WARMING

The contemporary distribution of TCs was likely established during the late Pliocene around 3 million years ago and has been slightly modulated since then by glacial cycles on orbital timescales, abrupt climate changes on millennial timescales, gradual aerosol variations, and volcanism on sub-decadal timescales. The warm Pliocene (atmospheric $CO_2$ ~400 ppm) and warmer Eocene (~1000 ppm) epochs likely produced TCs at significantly higher latitudes than the pre-industrial climate (~280 ppm). However, recent studies have been divided on whether twenty-first century levels of atmospheric $CO_2$ (400 – 1000 ppm)[152.] will indeed result in a continuation of the present poleward trend in TC activity, as implied by those warm past climates.

Since at least the 1970s, the planet's TC distribution has unambiguously altered, evidenced in a poleward migration in latitudes of peak TC intensity at a rate of ~1/2 degree

514 latitude per decade. This subtle but robust poleward shift has occurred during an expansion of
515 the tropics at approximately the same rate but during a period of stable latitudes of the ITCZ
516 and subtropical jet. During the 21st century, responding to increasing atmospheric $CO_2$, the
517 global ITCZ may become stronger but move closer to the equator (Fig. 6). The effects of this
518 change on low latitude TCs are ambiguous since a stronger ITCZ implies more convective
519 mesoscale disturbances that could form into TCs as well higher free tropospheric humidity to
520 fuel their intensification, but also implies less planetary vorticity available for them to acquire
521 rotation and axisymmetric structure. Furthermore, these longitudinally averaged changes are
522 dominated by the Pacific where the eastern equatorial Pacific warming pattern is expected to
523 emerge during the 21st century. This will have the effect of drawing some of TC genesis away
524 from the western and eastern Pacific towards the central Pacific. In the North Atlantic,
525 changes in the favourability of baroclinic non-traditional TC genesis, vertical wind shear, and
526 ITCZ changes will be controlled by polar-amplified ocean warming (favourable to TC
527 poleward shift) possibly moderated by AMOC weakening (generally favourable to TC
528 equatorward shift).

529 Further tropical expansion is likely, primarily driven by amplified warming in the
530 tropical troposphere's upper levels, but will be constrained by the patterns of surface
531 warming. Crucially, new modelling of TCs at the changing tropical-extratropical margin
532 suggests that genesis and intensification between 30- and 40-degrees latitudes could
533 contribute significantly to the TC climatology of the twenty-first century. However, deep-
534 tropical TCs will remain a critical feature of Earth's climate, most clearly following the
535 anticipated equatorward ITCZ shift. Thus, we conclude that TCs will likely occupy a broader
536 range of latitudes by the end of the twenty-first century than during the pre-industrial period
537 following equatorward ITCZ shifts and continued increasing midlatitude favourability. We
538 propose that the bleeding-edge research questions critical for addressing uncertainties in

539 twenty-first century TCs are all centred around evaluating dynamical links between TC's
540 convective mesoscale processes and the better understood large-scale warming sensitivities
541 of the atmosphere and ocean. Potential feedbacks from TCs to climate is another broad
542 avenue for research.

## FIGURES

## [FIGURE 1]

**Fig. 1 | Tropical cyclogenesis in weather and climate. a** Earth's atmosphere on 22/07/2017 from NASA EOSDIS[153.]. This day exhibits the most simultaneously existing tropical cyclones (TCs) in the satellite record. Tropical Storm Roke (peak intensity 40 mph), Sonca (40 mph), Kulap (45 mph) and Typhoon Noru (110 mph) are seen in the western subtropical North Pacific. In the eastern North Pacific, Hurricane Fernanda (145 mph), Tropical Storm Greg (60 mph), Hurricane Hilary (110 mph) and Hurricane Irwin (90 mph) at various development stages. **b** Schematic of traditional and baroclinically-enabled tropical cyclogenesis embedded into the large-scale flow and modulated by atmospheric dynamics (see Extended Data Figs. 1 and 2 for examples). ITCZ is an acronym for Intertropical Convergence Zone. Schematic style of the tropical mean circulation following ref [154.].

**[FIGURE 2]**

**Fig. 2 | Planetary-scale atmospheric circulation, precipitation, and TC activity. a** Seasonal mean precipitation and lower-tropospheric winds and first recorded positions of disturbances that develop into tropical cyclones (TCs), **b** upper-tropospheric winds and TC tracks, **c** normalised average zonal-mean track density 2000-2019 (red) and 1980-1999 (blue), and **d** track density linear trends (units: local TC passages per year). The 6.5 mm/day contour in panel **a** corresponds to the 90$^{th}$ percentile seasonal-mean precipitation and marks the region of tropical convection during the TC seasons. Underlying environmental fields from ref. [155.] and TC data from ref.[156.]. Seasonal averages are computed for months of peak TC activity: July, August, September and October in the northern hemisphere and January, February, and March in the southern hemisphere (methods).

**[FIGURE 3]**

**Fig. 3 | Changes in TC latitudinal distribution over geological timescales.** **a** Modern TC tracks as in Fig. 2b with blue curves corresponding to the period 1980-1999 and red to 2000-2019, **b** simulated PETM tracks[34.], and **c** changes in simulated seasonal-mean genesis potential relative to pre-industrial throughout the Cenozoic. In **c**, yellow dashes indicate shifts in hemispheres' maximum genesis potential latitudes while green/blue columns mark their upper and lower bounds (defined as latitudes of 25% drop-offs on either side of maxima). The data in **b** and **c** are based on GCM simulations[34.][43.][78.] and hold large uncertainties. Red circles indicate observed satellite era poleward TC migration[94.]. Pre-industrial TC lifetime maximum intensity latitudes are 18ºN and 16ºS. Given the wide range in twenty-first century projections (see text), no future estimates are plotted.

**[FIGURE 4]**

**Fig. 4 | Recent linear trends in key thermodynamic variables affecting tropical cyclones (TCs) and their genesis potential. a** SST trends. **b** Trends in TC potential intensity (see Box 1) are controlled by the product of **c** air-sea thermodynamic disequilibrium and **d** modified Carnot efficiency. Thermodynamic disequilibrium represents the main heat source for TCs. Trends in the modified Carnot efficiency depend on **a** SST and **f** TC outflow temperature. Carnot efficiency represents the maximum efficiency at which the atmosphere can use available heat to maintain TC winds (Box 1). **e** Trends in genesis potential. See methods for the calculation of these variables. As in Fig. 2, seasonal averages are computed for months of peak TC activity. Underlying environmental fields are from ERA5 data[155.]; trends are computed for 1980-2019. Only values with $p < 0.05$ are plotted.

**[FIGURE 5]**

**Fig. 5 | Large-scale circulations and TC latitudinal distributions under idealized climate warming scenarios in cloud-system-resolved aquaplanet simulations.** This model is forced by **a** three fixed sea surface temperature (SST) meridional profiles ranging from contemporary climate (blue) to moderate midlatitude warming (purple) to exaggerated Eocene-like warming (yellow). The plot shows **b** 20 m/s zonal velocity contours marking the jet streams, **c** ±30 x $10^9$ kg/s streamlines of the Hadley and Ferrel cells, and **d** mean updraft strength measured as the time-mean of the zonal minima pressure velocity at 500hPa multiplied by -1. Divergent influences lead to the northward shift of **e** TC life-time maximum intensity (LMI) distribution (despite non-monotopic changes at low latitudes). Data from ref.[32.], which also finds that GPI calculations underestimate the magnitude of midlatitude genesis response to warming.

**[FIGURE 6]**

**Fig. 6 | Changes in the northern hemisphere Intertropical Convergence Zone (ITCZ) under different warming scenarios in CMIP6. a** ITCZ intensity, **b** width, and **c** latitudinal position. For higher tropical SSTs climate models predict a stronger and broader ITCZ shifted toward the equator (Methods; see Extended Data Fig. 7. for changes in the southern hemisphere). Data from refs [157.] [158.] [159.] [160.] [161.] [162.] [163.] [164.] [165.] [166.] [167.] [168.] [169.] [170.] [171.] [172.] [173.].

**Box 1 | Elemental controls**

**Potential intensity**

Potential intensity (PI) theory[174.], the only extant analytical framework for TC's environmental dependences, states that TC strength is regulated by (1) the rate of oceanic heat extraction - mainly through evaporation, (2) frictional dissipation at the ocean surface, and (3) thermodynamic efficiency, also called Carnot efficiency (the normalised difference between ocean surface and TC outflow temperatures), see Methods. The Carnot efficiency concept from classical thermodynamics is modified in the context of TCs to incorporate additional heating due to frictional energy dissipation. An upper bound on TC wind speeds is inferred from this framework and computed in various ways from gridded climate data. PI theory predicted three decades ago that anthropogenic warming would increase PI in warmer climates[175.], increasing occurrence of intense TCs (as opposed to more TCs of all strengths). This expectation has now been validated in recent observational data[176.].

**Convective aggregations**

When PI is high enough and an aggregation of high entropy air has occurred, the necessary thermodynamic conditions for TC genesis are satisfied[4.]. High entropy, or alternatively high moist static energy (MSE), follows warm and moist air columns that are established by surface evaporation and sensible heat transfer, radiative fluxes, and horizontal advection. These aggregations may originate from a wide variety of synoptic and mesoscale disturbances with embedded convective systems: easterly waves, the barotropic breakdown of the ITCZ, convectively coupled equatorial waves, the Madden-Julian Oscillation (MJO), or the remnants of baroclinic activity in the midlatitudes (Fig. 1b). Convective self-aggregation may be another potentially important mechanism[2.][177.].

**Large-scale winds**

Environmental winds advect the developing vortex, thereby *steering* it, while interfering with its structure and energetics. Vertical wind variations, or *wind shear*, are intrinsic to all planetary atmospheres characterized by horizontal temperature gradients, leading to time-mean atmospheric features like low-level subtropical anticyclonic flows (Fig. 2a) and upper-level zonal jets (Fig. 1b; Fig. 2b). Vertical shear is the major dynamical inhibitor of TC intensification acting against the formation of coherent deep columns of high entropy air required for genesis. This shear dilutes entropy thereby weakening convective updrafts and slowing the surface winds required for extracting heat from the ocean to fuel continued convection[178.].

**Planetary rotation**

Two key scaling hypotheses exist for the dependence of TCs on the planet's rotation. Planetary rotation is manifest as the Coriolis parameter $f$ ($= 2\Omega sin\phi$, $\phi$ – latitude, $\Omega$ - rotation rate of the planet), also called planetary vorticity. A first hypothesis predicts an *f*-scaling, i.e., all else ignored, TCs should become more frequent towards the poles[141.]. The Coriolis parameter is zero at the equator and increases with latitude, setting a meridional vorticity gradient (Fig. 1b). This gradient, the so-called $\beta$-effect, is also relevant:

$$\beta = \frac{df}{dy} = \frac{2\Omega}{a} cos\phi. \qquad [1.]$$

Opposite to *f*, $\beta$ is largest at the equator and zero at the poles. This gradient is what causes TC to move poleward and westward (the process known as beta drift) by establishing secondary "beta gyre" circulations[179.] on either side of the TC (Fig. 1b). Beta drift scales with the square root of $\beta$[180.]. Consequently, TC westward tracks rapidly curve poleward in the tropics, but this effect diminishes at higher latitudes. $\beta$ provides a non-climatological (i.e., dependent on planetary size and rotation rate as opposed to mean climate) constraint on TC

latitudes by limiting the size of cyclonic disturbances and hence reducing beta drift. [143.]. If TC radii are to increase with climate warming, as has been hypothesised[100.], then we would expect stronger beta drift.

**Climatological Convection**

The majority of TCs (~70%) are spun out directly from climatological convection (Fig. 2a). The large-scale structure of this convection, including the ITCZ, can be deduced by combining two conceptual building blocks of tropical dynamics – convective quasi-equilibrium theory [181.] (CQE) and the weak temperature gradient approximation[182.] (WTG) – into a single framework[183.]. This framework provides an explanation for the structure of large-scale convective circulations resulting from time-mean spatial variations in MSE. CQE abstracts that the upward flow of MSE into the sub-cloud boundary layer due to enthalpy fluxes (latent and sensible heat transfer from the ocean surface) is balanced by a downward transfer of low MSE air from the dry free troposphere through convective downdrafts and large-scale subsidence (Fig. 1b). Employing this balance, ref.[183.] provides the following zeroth order diagnostic expression for controls on the strength of climatological convective updrafts in the ITCZ and Pacific Warm Pool:

$$M_u \propto w + \frac{SEF}{\Delta MSE}, \qquad [2.]$$

where $M_u$ is the mass flux of the deep convective updrafts, $w$ – the tropical average vertical velocity at the top of the boundary layer, $SEF$ – the surface moist enthalpy fluxes, and $\Delta MSE$ – the difference between the boundary layer $MSE$ and free tropospheric $MSE$ (per unit volume). The corresponding convective updrafts release local instabilities and transport $MSE$ from the boundary layer into the free troposphere. Eq. [2.] implies that the horizonal distribution of updraft strength is constrained by horizonal variations in surface fluxes, boundary layer $MSE$ and free tropospheric $MSE$. Since atmospheric moisture content

680 declines rapidly with altitude and the effect of latent heat flux dominates over sensible heat
681 flux, the spatial distribution of climatological convection largely reflects surface evaporative
682 fluxes and lower-level tropospheric moisture[184.].

## REFERENCES


[1.] Hsieh, T., Vecchi, G. A., Yang, W., Held, I. M. & Garner, S. T. Large-scale control on the frequency of tropical cyclones and seeds: a consistent relationship across a hierarchy of global atmospheric models. *Clim. Dyn.* **55**, 3177-3196 (2020). https://link.springer.com/article/10.1007/s00382-020-05446-5

[2.] Boos, W. R., Fedorov, A. & Muir. L. Convective self-aggregation and tropical cyclogenesis under the hypohydrostatic rescaling. *J. Atmos. Sci.* **73** (2), 525-544 (2016). https://journals.ametsoc.org/jas/article/73/2/525/27782

[3.] Emanuel, K.100 years of progress in tropical cyclone research. *Meteor. Monogr.* **59** : 15.1-15.68 (2018). https://journals.ametsoc.org/view/journals/amsm/59/1/amsmonographs-d-18-0016.1.xml

[4.] Tang, B. H. et al. Recent advances in research on tropical cyclogenesis. *Tropical Cyclone Research and Review*. **9**: 87-105 (2020). https://www.sciencedirect.com/science/article/pii/S2225603220300187

[5.] Shaw, N. The Birth and Death of Cyclones, p. 218: in Newnham E. V.: Hurricanes and Tropical Revolving Storms. *Geophysical Memoirs.* **19**; Met Office, London (1922). https://digital.nmla.metoffice.gov.uk/IO_8b3319c1-b2f3-47ce-a9c0-f77c445dad6f/

[6.] Knutson, T. et al. Tropical Cyclones and Climate Assessment: Part II: Projected Response to Anthropogenic Warming. *Bull. Amer. Meteor. Soc.,* **101**, E303–E322 (2020). https://doi.org/10.1175/BAMS-D-18-0194.1.

[7.] Gray, W. M. Hurricanes: Their formation, structure, and likely role in the tropical circulation. Meteorology over the Tropical Oceans, D. B. Shaw, Ed., *Royal Meteorological Society*, 155–218 (1979).

[8.] Emanuel, K., Ravela, S., Vivant, E. & Risi., C. A statistical deterministic approach to hurricane risk assessment. *BAMS.* **87** (3), 299-314 (2006). https://journals.ametsoc.org/view/journals/bams/87/3/bams-87-3-299.xml

[9.] Camargo, S., J. & Wing, A. A. Tropical cyclones in climate models. *Wires Climate Change.* **7** (2), 211-237 (2016). https://onlinelibrary.wiley.com/doi/abs/10.1002/wcc.373

[10.] Emanuel, K. Downscaling CMIP5 climate models shows increased tropical cyclone activity over the 21st century. *PNAS.* **110** (30), 12219-12224 (2013). https://www.pnas.org/content/110/30/12219

[11.] Emanuel, K. Response of global tropical cyclone activity to increasing CO2: results from downscaling CMIP6 models. J. Climate. 34 (1). 57-70 (2021). https://journals.ametsoc.org/view/journals/clim/34/1/jcliD200367.xml

[12.] Knutson, T. R. et al. Global Projections of Intense Tropical Cyclone Activity for the Late Twenty-First Century from Dynamical Downscaling of CMIP5/RCP4.5 Scenarios. J. Climate, 28, 7203–7224 (2015). https://journals.ametsoc.org/jcli/article/28/18/7203/34019/Global-Projections-of-Intense-Tropical-Cyclone

[13.] Roberts, M. J. et al. Projected future changes in tropical cyclones using the CMIP6 HighResMIP Multimodel Ensemble. Geophysical Research Letters. 47, e2020GL088662 (2020). https://agupubs.onlinelibrary.wiley.com/doi/full/10.1029/2020GL088662

[14.] Vidale, P. L. et al. Impact of stochastic physics and model resolution on the simulation of tropical cyclones in climate GCMs. *J. Climate.* **34** (11), 4315-4341 (2021). https://journals.ametsoc.org/view/journals/clim/aop/JCLI-D-20-0507.1/JCLI-D-20-0507.1.xml

[15.] Lee, C.-Y., Camargo, S. J., Sobel, A. H. & Tippett, M. K. Statistical-dynamical downscaling projections of tropical cyclone activity in a warming climate: two diverging genesis scenarios. *J. Climate.* **33**(11), 4815-4834 (2020). https://journals.ametsoc.org/jcli/article/33/11/4815/345277/Statistical-Dynamical-Downscaling-Projections-of

[16.] Vecchi, G. A. et al. Tropical cyclone sensitivities to CO2 doubling: roles of atmospheric resolution, synoptic variability and background climate changes. *Climate Dynamics.* **53** : 5999-6033 (2019). https://link.springer.com/article/10.1007/s00382-019-04913-y

[17.] Camargo, S. J. et al. Characteristics of Model Tropical Cyclone Climatology and the Large-Scale Environment. *J. Climate*, **33**, 4463–4487 (2020). https://journals.ametsoc.org/jcli/article/33/11/4463/345276/Characteristics-of-Model-Tropical-Cyclone

[18.] Sugi, M. et al. Future changes in the global frequency of tropical cyclone seeds. *SOLA*, **16**, 70-74 (2020). https://www.jstage.jst.go.jp/article/sola/16/0/16_2020-012/_article

[19.] Ramsay, H. A., Singh, M. S. & Chavas, D. R. Response of tropical cyclone formation and intensification rates to climate warming in idealised simulations. *JAMES.* **12** (10), e2020MS002086 (2020). https://agupubs.onlinelibrary.wiley.com/doi/full/10.1029/2020MS002086

[20.] Yamada, Y. et al. Evaluation of the contribution of tropical cyclone seeds to changes in tropical cyclone frequency due to global warming in high-resolution multi-model ensemble simulations. *Progress in Earth and Planetary Sciences.* **8** (11) (2021). https://progearthplanetsci.springeropen.com/articles/10.1186/s40645-020-00397-1

[21.] Knutson, T. R. et al. Tropical cyclones and climate change. *Nature Geoscience.* **3,** 157-163 (2010). https://www.nature.com/articles/ngeo779

[22.] Walsh, K. J. E. et al. Tropical cyclones and climate change. *WIRES Clim. Chang*., **7**, 65-89 (2016). https://onlinelibrary.wiley.com/doi/epdf/10.1002/wcc.371

[23.] Merlis, T. M., & Held, I. M. Aquaplanet simulations of Tropical Cyclones, *CCCR.* **5** : 185-195 (2019). https://link.springer.com/article/10.1007/s40641-019-00133-y

[24.] Chen, H.-F. et al. China's historical record when searching for tropical cyclones corresponding to Intertropical Convergence Zone (ITCZ) shifts over the past 2 kyr. *Clim. Past*. **15,** 279-289 (2019). https://cp.copernicus.org/articles/15/279/2019/

[25.] Pausata, F. S. R., & Camargo, S. J. Tropical cyclone activity affected by volcanically induced ITCZ shifts. *PNAS*. **116**(16), 7732-7737 (2019). https://www.pnas.org/content/116/16/7732

[26.] McTaggart-Cowan, R., Galarneau Jr., T. J., Bosart L. F., Moore, R. W., & Martius, O. A global climatology of baroclinically influenced tropical cyclogenesis. *Mon. Wea. Rev.* **141** (6): 1963-1989 (2013). https://journals.ametsoc.org/mwr/article/141/6/1963/71760/A-Global-Climatology-of-Baroclinically-Influenced

[27.] Davis, C. A., & Bosart, L. F. Baroclinically induced tropical cyclogenesis. *Mon. Wea Rev.* **131** (11), 2730-2747 (2003). https://journals.ametsoc.org/mwr/article/131/11/2730/67174/Baroclinically-Induced-Tropical-Cyclogenesis

[28.] Bentley, A. M., & Metz, N. D. Tropical transition of an unnamed, high-latitude, tropical cyclone over the Eastern North Pacific. *Mon. Wea. Rev.* **144** (2), 713-736 (2016). https://journals.ametsoc.org/mwr/article/144/2/713/72262

783 [29.] Thorncroft, C. D., Hoskins, B. J., & McIntyre, M. E. Two paradigms of baroclinic-wave
784 life-cycle behaviour, *Q. J. Met. Roy. Soc*. **119** (509), 17-55 (1993).
785 https://rmets.onlinelibrary.wiley.com/doi/10.1002/qj.49711950903
786 [30.] Romero, R., & Emanuel, K. Climate change and hurricane-like extratropical cyclones:
787 Projections for North Atlantic polar lows and medicanes based on CMIP5
788 models. *J. Climate*. **30** (1), 279-299 (2017).
789 https://journals.ametsoc.org/view/journals/clim/30/1/jcli-d-16-
790 0255.1.xml?tab_body=fulltext-display
791 [31.] Korty, R. L., Emanuel, K. E., Huber, M., & Zamora, R. A. Tropical Cyclones
792 Downscaled from Simulations with Very High Carbon Dioxide Levels. *J.*
793 *Climate*. **30**:649-667 (2017).
794 https://journals.ametsoc.org/jcli/article/30/2/649/96160/Tropical-Cyclones-
795 Downscaled-from-Simulations-with
796 [32.] Fedorov, A., Muir, L., Boos, W. R., & Studholme, J. Tropical cyclogenesis in warm
797 climates simulated by a cloud-system resolving model. *Climate Dyn*., **52**, 107-
798 127 (2019). https://link.springer.com/article/10.1007/s00382-018-4134-2
799 [33.] Zhang, G., Silvers, L. G., Zhao, M., & Knutson, T. R. Idealized aquaplanet simulations of
800 tropical cyclone activity: significance of temperature gradients, Hadley
801 circulation, and zonal asymmetry. *J. Atmos. Sci.* **78** (3), 877-902 (2021).
802 https://journals.ametsoc.org/view/journals/atsc/aop/JAS-D-20-0079.1/JAS-D-20-
803 0079.1.xml
804 [34.] Kiehl, J. T., Zarzycki, C. M., Shields, C. A., & Rothstein, M. V. Simulated changes to
805 tropical cyclones across the Paleocene-Eocene Thermal Maximum (PETM)
806 boundary. *Paleogeography, Paleoclimatology, Palaeoecology*. **572**, 110421
807 (2021). https://www.sciencedirect.com/science/article/pii/S0031018221002066

[35.] Yang, G.-Y., Methven, J., Woolnough, S., Hodges, K., & Hoskins, B. Linking African Easterly Wave activity with Equatorial Waves and the influence of Rossby Waves from the Southern Hemisphere. *J. Atmos. Sci.* **75** (6), 1783-1809 (2018). https://journals.ametsoc.org/jas/article/75/6/1783/107259/Linking-African-Easterly-Wave-Activity-with

[36.] Russell, J. O., Aiyyer, A., White, J. D. & Hannah, W. Revisiting the connection between African Easterly Waves and Atlantic tropical cyclogenesis. *GRL***. 44** (1), 587-595 (2017). https://agupubs.onlinelibrary.wiley.com/doi/full/10.1002/2016GL071236

[37.] Wu, L. & Takahashi, M. Contributions of tropical waves to tropical cyclone genesis over the western North Pacific. *Climate Dynamics*. **50**, 4635-4649 (2018). https://link.springer.com/article/10.1007/s00382-017-3895-3

[38.] Thorncroft, C. D. & Hodges, K. I. 2001: African easterly wave variability and its relationship to Atlantic tropical cyclone activity. *J. Climate.* **14,** 1166-1179 (2001). https://journals.ametsoc.org/jcli/article/14/6/1166/29821/African-Easterly-Wave-Variability-and-Its

[39.] Patricola, C. M., Saravanan, R., & Chang, P. The response of Atlantic tropical cyclones to suppression of African easterly waves. *Geophys. Res. Lett*. **45** (1): 471-479 (2018). https://agupubs.onlinelibrary.wiley.com/doi/full/10.1002/2017GL076081

[40.] Sardeshmukh, P. D. & Hoskins, B. J. The generation of global rotational flow by steady idealised tropical divergence. *J. Atmos. Sci*. **45** (7). 1228-1251 (1988). https://journals.ametsoc.org/jas/article/45/7/1228/21914/The-Generation-of-Global-Rotational-Flow-by-Steady

[41.] Tang, B. H. & Neelin, D. J. ENSO influence on Atlantic hurricanes via tropospheric warming. *Geophy. Res. Lett.*, **31** (24) (2004). https://agupubs.onlinelibrary.wiley.com/doi/full/10.1029/2004GL021072

[42.] Vecchi, G. A. & Soden, B. J. Effect of remote sea surface temperature change on tropical cyclone potential intensity. *Nature.* **450**, 1066-1070 (2007). https://www.nature.com/articles/nature06423

[43.] Yan, Q., Korty, R., Zhang, Z. & Wang, H. Evolution of tropical cyclone genesis regions during the Cenozoic era. *Nature Communications*. **10**, 3076 (2019). https://www.nature.com/articles/s41467-019-11110-2

[44.] Anagnostou, E., John, E. H., Edgar, K. M. & co-authors. Changing atmospheric $CO_2$ concentration was the primary driver of early Cenozoic climate. *Nature.* **533**, 380-384 (2016). https://www.nature.com/articles/nature17423.pdf

[45.] Evans, D. et al. Eocene greenhouse climate revealed by coupled clumped isotope-Mg/Ca thermometry. *PNAS.* **115** (6), 1174-1179 (2018). https://www.pnas.org/content/pnas/115/6/1174.full.pdf

[46.] Cramwinckel, M. J. et al. Synchronous tropical and polar temperature evolution in the Eocene. *Nature.* **559**, 382-386 (2018). https://www.nature.com/articles/s41586-018-0272-2

[47.] Van Dijk, J. et al. Spatial pattern of super-greenhouse warmth controlled by elevated specific humidity. *Nature Geoscience.* **13**, 739-744 (2020). https://www.nature.com/articles/s41561-020-00648-2.pdf

[48.] Evans, D., Wade, B. S., Henehan, M., Erez, J. & Muller, W. Revisiting carbonate chemistry controls on planktic foraminifera Mg / Ca: implications for sea surface temperature and hydrology shifts over the Paleocene-Eocene Thermal Maximum and Eocene-Oligocene transition. *Clim. Past.* **12**, 819-835 (2016). https://cp.copernicus.org/articles/12/819/2016/

[49.] Frieling, J. et al. Extreme warmth and heat-stressed plankton in the tropics during the Paleocene-Eocene Thermal Maximum. *Science Advances*. **3**(3), e1600891 (2017). https://advances.sciencemag.org/content/3/3/e1600891

[50.] Huber, M. & Caballero, R. The early Eocene equable climate problem. *Clim. Past.* **7**, 603-633 (2011). https://cp.copernicus.org/articles/7/603/2011/

[51.] Carmichael, M. J. et al. A model-model and data-model comparison for the early Eocene hydrological. *Clim. Past.* **12**, 455-481 (2016). https://cp.copernicus.org/articles/12/455/2016/cp-12-455-2016.pdf

[52.] Baatsen, M. et al. The middle to late Eocene greenhouse climate modelled using the CESM 1.0.5. *Clim. Path.* **16**, 2573-2597 (2020). https://cp.copernicus.org/articles/16/2573/2020/cp-16-2573-2020.pdf

[53.] Lunt, D. J. et al. DeepMIP: model intercomparison of early Eocene climate optimum (EECO) large-scale climate features and comparison with proxy data. *Clim. Past.* **17**, 203-227 (2021). https://cp.copernicus.org/articles/17/203/2021/cp-17-203-2021.pdf

[54.] Fedorov, A. V., Brierley, C. M., & Emanuel, K. E. Tropical cyclones and permanent El Niño in the early Pliocene epoch. *Nature*. **463**, 1066-1070 (2010). https://www.nature.com/articles/nature08831

[55.] Martínez-Botí, M. A et al. Plio-Pleistocene climate sensitivity evaluated using high-resolution $CO_2$ records. *Nature.* **518**, 49-54 (2015). https://www.nature.com/articles/nature14145#auth-M__A_-Mart_nez_Bot_

[56.] Fedorov, A. V. et al. Patterns and mechanisms of early Pliocene warmth. *Nature.* **496**, 43-49 (2013). https://www.nature.com/articles/nature12003

[57.] Abell, J. T., Winckler, G., Anderson, R. F. & Herbert, T. D. 2021: Poleward and weakened westerlies during Pliocene warmth. *Nature*. **589**, 70-74 (2021). https://www.nature.com/articles/s41586-020-03062-1.pdf

[58.] Brierley, C. M. et al. Greatly expanded tropical warm pool and weakened Hadley circulation in the early Pliocene. *Science*. **323** (5922). 1714-1718 (2009). https://science.sciencemag.org/content/323/5922/1714.abstract

[59.] Yan, Q. et al. Enhanced intensity of global tropical cyclones during the mid-Pliocene warm period. *PNAS*, **113**: 12963–12967 (2016). https://www.pnas.org/content/113/46/12963

[60.] Haywood, A. M. et al. The Pliocene Model Intercomparison Project Phase 2: large-scale climate features and climate sensitivity. *Clim. Past.* **16**, 2095-2123 (2020). https://cp.copernicus.org/articles/16/2095/2020/cp-16-2095-2020.pdf

[61.] Haug, G. H., Sigman, D. M., Tiedemann, R., Pedersen, T. F. & Sarnthein, M. Onset of permanent stratification in the subarctic Pacific Ocean. *Nature*. **401**, 779-782 (1999). https://www.nature.com/articles/44550

[62.] Hobgood, J. S. & Cerveny, R. S. Ice-age hurricanes and tropical storms. *Nature*. **333**, 243-245 (1988). https://www.nature.com/articles/333243a0

[63.] Yoo, J., Galewsky, J., Camargo, S. J., Korty, R. & Zamora, R. Dynamical downscaling of tropical cyclones from CCSM4 simulations of the Last Glacial Maximum. *JAMES*. **8,** 1229-1247 (2016). https://agupubs.onlinelibrary.wiley.com/doi/epdf/10.1002/2016MS000685

[64.] Lawton, Q. A., Korty, R. L. & Zamora, R. A. Tropical cyclones downscaled from simulations of the Last Glacial Maximum. *J. Climate*. **34**(2), 659-674 (2021). https://journals.ametsoc.org/view/journals/clim/aop/jcliD200409/jcliD200409.xml

[65.] Harrison, S. P. et al. Climate model benchmarking with glacial and mid-Holocene climates. *Climate Dynamics.* **43**, 671-688 (2014). https://link.springer.com/article/10.1007%2Fs00382-013-1922-6

[66.] Harrison, S. P. et al. Evaluations of CMIP5 palaeo-simulations to improve climate projections. *Nature Climate Change.* **5**, 735-743 (2015). https://www.nature.com/articles/nclimate2649

[67.] Yan, Q. & Zhang, Z. Dominating roles of ice sheets and insolation in variation of tropical cyclone genesis potential over the North Atlantic during the last 21,000 years. *GRL*, **44**:10624–10632 (2017). https://agupubs.onlinelibrary.wiley.com/doi/full/10.1002/2017GL075786

[68.] Boos, W. R. & Korty, R. L. Regional energy budget control of the intertropical convergence zone and application to mid-Holocene rainfall. *Nature Geoscience.* **9**, 892-897 (2016). https://www.nature.com/articles/ngeo2833.pdf

[69.] Adam, O., Schneider, T., Enzel, Y., & Quade, J. Both differential and equatorial heating contributed to African monsoon variations during the mid-Holocene. *Earth and Planetary Science Letters.* **522**, 20-29 (2019). https://www.sciencedirect.com/science/article/pii/S0012821X19303589

[70.] Lamy, F. et al. Precession modulation of the South Pacific westerly wind belt over the past million years. *PNAS.* **116**, 23455-23460 (2019). https://www.pnas.org/content/116/47/23455

[71.] Routson, C. et al. Mid-latitude net precipitation decreased with Arctic warming during the Holocene. *Nature.* **568**, 83-87 (2019). https://www.nature.com/articles/s41586-019-1060-3

927 [72.] Henry, L. G. et al. North Atlantic Ocean circulation and abrupt climate change during the
928 last glaciation. *Science.* **353**, 470-474 (2016).
929 https://science.sciencemag.org/content/353/6298/470
930 [73.] McGee, D., Moreno-Chamarro, E., Marshall, J. & Galbraith, E. D. Western U.S. lake
931 expansions during Heinrich stadials linked to Pacific Hadley circulation. *Science*
932 *Advances.* **4**, eaav0118 (2018).
933 https://advances.sciencemag.org/content/4/11/eaav0118
934 [74.] Yang, Y., et al. Latitudinal response of storm activity to abrupt climate change during the
935 last 6,500 years. *GRL.* **47**, e2020GL089859 (2020).
936 https://agupubs.onlinelibrary.wiley.com/doi/epdf/10.1029/2020GL089859
937 [75.] McGee, D., Donohoe, A., Marshall, J., & Ferreira, D. Changes in ITCZ location and
938 cross-equatorial heat transport at the Last Glacial Maximum, Heinrich Stadial 1,
939 and the mid-Holocene. *Earth and Planetary Science Letters.* **390**, 69-79 (2014).
940 https://www.sciencedirect.com/science/article/pii/S0012821X13007589
941 [76.] Pausata, F. S. R. et al. Tropical cyclone activity enhanced by Sahara greening and
942 reduced dust emissions during the African Humid Period. *PNAS.* **114** (24) 6221-
943 6226 (2017). https://www.pnas.org/content/114/24/6221
944 [77.] Dandoy, S. et al. Atlantic hurricane response to Saharan greening and reduced dust
945 emissions during the mid-Holocene. *Clim. Past.* **17**, 675-701 (2021).
946 https://cp.copernicus.org/articles/17/675/2021/cp-17-675-2021.pdf
947 [78.] Korty, R. L., Camargo, S. J. & Galewsky, J. Variations in tropical cyclone genesis factors
948 in simulations of the Holocene epoch. *J. Climate*, **25**, 8196–8211 (2012).
949 https://journals.ametsoc.org/jcli/article/25/23/8196/33763/Variations-in-Tropical-
950 Cyclone-Genesis-Factors-in

951 [79.] Evans S., Dawson, E. & Ginoux, P. Linear relation between shifting ITCZ and dust
952 hemispheric asymmetry. *GRL*. **47**. E2020GL090499 (2020).
953 https://agupubs.onlinelibrary.wiley.com/doi/epdf/10.1029/2020GL090499
954 [80.] Yan, Q., Korty, R. & Zhang, Z. Tropical cyclone genesis factors in a simulation of the
955 last two millennia: Results from the Community Earth System Model. *J. Climate.*
956 **28** (18), 7182–7202 (2015).
957 https://journals.ametsoc.org/jcli/article/28/18/7182/34021/Tropical-Cyclone-
958 Genesis-Factors-in-a-Simulation
959 [81.] Baldini, L. M. et al. Persistent northward North Atlantic tropical cyclone track migration
960 over the past five centuries. *Scientific Reports*, **6**: 37 522 (2016).
961 https://www.nature.com/articles/srep37522.
962 [82.] Donnelly, J. P. et al. Climate forcing of unprecedented intense-hurricane activity in the
963 last 2000 years. *Earth's Future*, **3**(2) : 49–65 (2015).
964 https://agupubs.onlinelibrary.wiley.com/doi/full/10.1002/2014EF000274
965 [83.] Mann, M. E., Woodruff, J. D., Donnelly, J. P. & Zhang, Z. Atlantic hurricanes and
966 climate over the past 1,500 years. *Nature*, **460**(7257): 880–883 (2009).
967 https://www.nature.com/articles/nature08219
968 [84.] Bramante, J. F. et al. Increased typhoon activity in the Pacific deep tropics driven by
969 Little Ice Age circulation changes. *Nature Geoscience*. **13**, 806-811 (2020).
970 https://www.nature.com/articles/s41561-020-00656-2
971 [85.] Rustic, G. T., Koutavas, A., Marchitto, T. M. & Linsley, B. K. Dynamical excitation of
972 the tropical Pacific Ocean and ENSO variability by Little Ice Age cooling.
973 *Science.* **350** (6267) 1537-1541 (2015).
974 https://science.sciencemag.org/content/350/6267/1537

975 [86.] Altman, J. et al. Poleward migration of the destructive effects of tropical cyclones during
976 the 20th century. *Proceedings of the National Academy of Sciences*, **115** (45)
977 11543-11548 (2018). https://www.pnas.org/content/115/45/11543
978 [87.] Donnelly, J. P. & Woodruff, J. D. Intense hurricane activity over the past 5,000 years
979 controlled by El Niño and the West African monsoon. *Nature*, 447: 465–468
980 (2007). https://www.nature.com/articles/nature05834
981 [88.] Hernandez, A. et al. Modes of climate variability: Synthesis and review of proxy-based
982 reconstructions through the Holocene. *Earth-Science Reviews*. **209** 103286
983 (2020). https://www.sciencedirect.com/science/article/pii/S0012825220303329
984 [89.] Van Hengstum, P. J. et al. The intertropical convergence zone modulates intense
985 hurricane strikes on the western North Atlantic margin. *Scientific Reports*. **6**:
986 21728 (2016).
987 https://www.nature.com/articles/srep21728#:~:text=Here%20we%20present%20
988 a%203000,on%20millennial%20to%20centennial%2Dscales.
989 [90.] Liu, K.-B & Fearn, M. L. Reconstruction of prehistoric landfall frequencies of
990 catastrophic hurricanes in northwestern Florida from lake sediment records.
991 *Quaternary Research.* **54**, 238-245 (2000).
992 https://www.sciencedirect.com/science/article/pii/S0033589400921665
993 [91.] Liu, K.-B & Fearn, M. L. Lake-sediment record of late Holocene hurricane activities
994 from coastal Alabama. *Geology.* **21** (9). 793-796 (1993).
995 https://pubs.geoscienceworld.org/gsa/geology/article/21/9/793/185986/Lake-
996 sediment-record-of-late-Holocene-hurricane
997 [92.] Wallace, E. J., Coats, S., Emanuel, K. & Donnelly, J. P. Centennial-scale shifts in storm
998 frequency captured in paleohurricane records from the Bahamas arise

predominately from random variability. *GRL*. **47**, e2020GL091145 (2020). https://agupubs.onlinelibrary.wiley.com/doi/epdf/10.1029/2020GL091145

[93.] Wallace, E. J. et al. Intense hurricane activity over the past 1500 years at South Andros Island, The Bahamas. *Paleooceanography and Paleoclimatology*. **34**, 1761-1783 (2019). https://agupubs.onlinelibrary.wiley.com/doi/epdf/10.1029/2019PA003665

[94.] Kossin, J. P., Emanuel, K. & Vecchi, G. A. The poleward migration of the location of tropical cyclone maximum intensity. *Nature*, **509** (7500), 349–352 (2014). http://www.nature.com/doifinder/10.1038/nature13278.

[95.] Daloz, A. S. & Camargo, S. J. Is the poleward migration of tropical cyclone maximum intensity associated with a poleward migration of tropical cyclone genesis? *Climate Dynamics*, **50** (1-2), 705–715 (2018). https://link.springer.com/article/10.1007/s00382-017-3636-7

[96.] Studholme, J. & Gulev, S. Concurrent changes to Hadley circulation and the meridional distribution of tropical cyclones. *J. Climate*. **31**(11): 4367-4389 (2018). https://journals.ametsoc.org/jcli/article/31/11/4367/94654

[97.] Hodges, K., Cobb, A. & Vidale, P. L. How well are tropical cyclones represented in reanalysis datasets. *J. Climate.* **30** (14), 5243-5264 (2017). https://journals.ametsoc.org/jcli/article/30/14/5243/96967/How-Well-Are-Tropical-Cyclones-Represented-in

[98.] Wang, C., Wang, L., Wang, X., Wang, D. & Wu, L. North-south variations of tropical storm genesis locations in the Western Hemisphere. *Geophysical Research Letters.* **43:** 11367-11374 (2016). https://agupubs.onlinelibrary.wiley.com/doi/full/10.1002/2016GL071440

[99.] Sharmila, S. & Walsh, K. J. E. Recent poleward shift of tropical cyclone formation linked to Hadley cell expansion. *Nature Climate Change*. **8**, 730-736 (2018). https://www.nature.com/articles/s41558-018-0227-5

[100.] Sun, Y. et al. Impact of Ocean Warming on Tropical Cyclone Size and Its Destructiveness. *Scientific Reports*. **7**, 8154 (2017). https://www.nature.com/articles/s41598-017-08533-6

[101.] Zhan, R. & Wang, Y. Weak tropical cyclones dominate the poleward migration of the annual mean location of lifetime maximum intensity of northwest Pacific tropical cyclones since 1980. *J. Climate*., **30**, 6873–6882 (2017). https://journals.ametsoc.org/doi/pdf/10.1175/JCLI-D-17-0019.1

[102.] Mokhov, I. I., Makarova, and A. G. Poroshenko. Tropical cyclones and their transformation into extratropical: estimates of the half-century trends. Physics of Atmosphere. 493 (1), 83-88. https://link.springer.com/article/10.1134/S1028334X20070107

[103.] Kossin, J. P., Emanuel, K. & Camargo, S. J. Past and projected changes in western north pacific tropical cyclone exposure. *J. Clim*. **29** (16), 5725–5739 (2016). https://journals.ametsoc.org/jcli/article/29/16/5725/107101/Past-and-Projected-Changes-in-Western-North

[104.] Song, J. & Klotzbach, P. J. What Has Controlled the Poleward Migration of Annual Averaged Location of Tropical Cyclone Lifetime Maximum Intensity Over the Western North Pacific Since 1961? *Geophysical Research Letters*, **45** (2), 1148–1156 (2018). doi:10.1002/2017GL076883. https://agupubs.onlinelibrary.wiley.com/doi/full/10.1002/2017GL076883

[105.] Vecchi, G. A. & Soden, B. J. Increased tropical Atlantic wind shear in model projections of global warming. *GRL.* **34,** L08702 (2007). https://agupubs.onlinelibrary.wiley.com/doi/full/10.1029/2006GL028905

[106.] Bell, S. S., Chand, S. S. & Turville, C. Projected changes in ENSO-driven regional tropical cyclone tracks. *Climate Dynamics*. **54**, 2533-2559 (2020). https://link.springer.com/article/10.1007/s00382-020-05129-1

[107.] Zhang, L. & Karnauskas, K. B. The role of tropical interbasin SST gradients in forcing Walker circulation trends. *J. Climate.* **30** (2), 499-508 (2017). https://journals.ametsoc.org/jcli/article/30/2/499/95964/The-Role-of-Tropical-Interbasin-SST-Gradients-in

[108.] Hu, S. & Fedorov, A. V. Cross-equatorial winds control El Niño diversity and change. *Nature Climate Change.* **8**, 798-802 (2018). https://www.nature.com/articles/s41558-018-0248-0

[109.] Heede, U. & Fedorov, A. Eastern equatorial Pacific warming delayed by aerosols and thermostat response to $CO_2$. Preprint at *https://www.researchsquare.com/article/rs-133479/v1* (2021)

[110.] Zhang, W. et al. Dominant Role of Atlantic Multidecadal Oscillation in the Recent Decadal Changes in Western North Pacific Tropical Cyclone Activity. *Geophysical Research Letters.* **45:**354-362 (2018). https://agupubs.onlinelibrary.wiley.com/doi/full/10.1002/2017GL076397

[111.] Zhao, B. & Fedorov, A. The seesaw response of the intertropical and South Pacific convergence zones to hemispherically asymmetric thermal forcing. *Climate Dynamics.* **54**, 1639-1653 (2020). https://link.springer.com/article/10.1007/s00382-019-05076-6

[112.] Retsch M. H., Mauritsen, T. & Hohnegger, C. Climate change feedbacks in aquaplanet experiments with explicit parameterised convection for horizontal resolutions of 2,525 up to 5 km. *Journal of Advances in Modeling Earth Systems*. **11**, 2070-2088 (2019). https://agupubs.onlinelibrary.wiley.com/doi/full/10.1029/2019MS001677

[113.] Merlis, T. M., Zhao, M. & Held, I. M. The sensitivity of hurricane frequency to ITCZ changes and radiatively forced warming in aquaplanet simulations. *GRL*. **40** (15), 4109-4114 (2013). https://agupubs.onlinelibrary.wiley.com/doi/full/10.1002/grl.50680

[114.] Walsh, K. J. E. et al. Real world and tropical cyclone world. Part II: sensitivity of tropical cyclone formation to uniform and meridionally varying sea surface temperatures under aquaplanet conditions. *J. Climate*. **33**(4): 1473-1486 (2020). https://journals.ametsoc.org/jcli/article/33/4/1473/346333/Real-World-and-Tropical-Cyclone-World-Part-II

[115.] Emanuel, K., Sundararajan, R. & Williams, J. Hurricanes and global warming: results from downscaling IPCC AR4 simulations. *BAMS.* **89** (3), 347-368 (2008). https://journals.ametsoc.org/bams/article/89/3/347/59287/Hurricanes-and-Global-Warming-Results-from

[116.] Bell, R., Strachan, J., Vidale, P. L., Hodges, K. & Roberts, M. Response of Tropical Cyclones to Idealized Climate Change Experiments in a Global High-Resolution Coupled General Circulation Model. *J. Climate*. **26,** 7966–7980 (2013). https://journals.ametsoc.org/jcli/article/26/20/7966/33735/Response-of-Tropical-Cyclones-to-Idealized-Climate

[117.] Murakami, H., Delworth, T. L., Cooke, W. F., Zhao, M., & Xiang, B. Detected climatic change in global distribution of tropical cyclones. *PNAS*. **117**(20), 10706-10714 (2020). https://www.pnas.org/content/117/20/10706

[118.] Bell, S. S. et al. Western North Pacific Tropical Cyclone Tracks in CMIP5 Models: Statistical Assessment Using a Model-Independent Detection and Tracking Scheme. *J. Climate*. **32:** 7191-7208 (2019). https://journals.ametsoc.org/jcli/article/32/21/7191/344453/Western-North-Pacific-Tropical-Cyclone-Tracks-in

[119.] Bell, S. S. et al. Projections of southern hemisphere tropical cyclone track density using CMIP5 models. *Climate Dynamics*. **52** : 6065–6079 (2019). https://link.springer.com/article/10.1007%2Fs00382-018-4497-4

[120.] Tang, B. & Camargo, S. J. Environmental control of tropical cyclones in CMIP5: a ventilation perspective. *JAMES.* **6** (1), 115-128 (2014). https://agupubs.onlinelibrary.wiley.com/doi/full/10.1002/2013MS000294

[121.] Li, T. et al. 2010: Global warming shifts Pacific tropical cyclone location. *Geophysical Research Letters*. **37**, L21804 (2010). https://agupubs.onlinelibrary.wiley.com/doi/full/10.1029/2010GL045124

[122.] Chu, J.-E. et al. Reduced tropical cyclone densities and ocean effects due to anthropogenic greenhouse warming. *Sci. Adv*. **6** (51), eabd5109 (2020). https://advances.sciencemag.org/content/6/51/eabd5109

[123.] Murakami, H., Wang, B., Li, T. & Kitoh, A. Projected increase in tropical cyclones near Hawaii, *Nature Climate Change*. **3**, 749-754 (2013). https://www.nature.com/articles/nclimate1890

[124.] Nakamura, J. et al. Western North Pacific Tropical Cyclone Model Tracks in Present and Future Climates. *Journal of Geophysical Research: Atmospheres*, **122**: 9721–

9744 (2017). https://agupubs.onlinelibrary.wiley.com/doi/10.1002/2017JD027007

[125.] Liu, M., Vecchi, G. A., Smith, J. A. & Murakami, H. The present-day simulation and twenty-first century projection of the climatology of extratropical transition in the North Atlantic. *J. Climate*. **30** (8), 2739-2756 (2017). https://journals.ametsoc.org/jcli/article/30/8/2739/95106/The-Present-Day-Simulation-and-Twenty-First

[126.] Michaelis, A. C. & Lackmann, G. M. Climatological changes in the extratropical transition of tropical cyclones in high-resolution global simulations. *J. Climate*. **32** (24), 8733-8753 (2019). https://journals.ametsoc.org/jcli/article-abstract/32/24/8733/344151/Climatological-Changes-in-the-Extratropical?redirectedFrom=fulltext

[127.] Jung, C. & Lackmann, G. M. 2021: The response of extratropical transition of tropical cyclones to climate change: Quasi-idealized numerical experiments. *J. Climate.* **34** (11), 4361-4381 (2021). https://journals.ametsoc.org/view/journals/clim/aop/JCLI-D-20-0543.1/JCLI-D-20-0543.1.xml

[128.] Zhang, G., Murakami, H., Knutson, T. R., Mizuta, R. & Yoshida, K. Tropical cyclone motion in a changing climate. *Sci. Adv.* **6** (17), eaaz7610 (2020). https://advances.sciencemag.org/content/6/17/eaaz7610

[129.] Camargo, S. Global and regional aspects of tropical cyclone activity in CMIP5 models. *J. Climate*. **26,** 9880-9902 (2013). https://journals.ametsoc.org/jcli/article/26/24/9880/33193/Global-and-Regional-Aspects-of-Tropical-Cyclone

1141 [130.] Wang, C., Zhang, L., Lee, S.-K., Wu. L. & Mechoso, C. R. A global perspective on
1142 CMIP5 climate model biases. *Nature Climate Change*. **4,** 201-205 (2014).
1143 https://www.nature.com/articles/nclimate2118
1144 [131.] Byrne, M. P., Pendergrass, A. G., Rapp. A. D. & Wodzicki, K. R. Response of the
1145 Intertropical Convergence Zone to climate change: location, width, and strength.
1146 *Current Climate Change Reports.* **4,** 355-370 (2018).
1147 https://link.springer.com/article/10.1007/s40641-018-0110-5
1148 [132.] Staten, P. W., Lu, J., Grise, K. M., Davis, S. M. & Birner, T. Re-examining tropical
1149 expansion. *Nature Climate Change*, **8** (9), 768– 775 (2018).
1150 https://www.nature.com/articles/s41558-018-0246-2.
1151 [133.] Shaw, T. A. Mechanisms of future predicted changes in the zonal mean mid-latitude
1152 circulation. *Current Climate Change Reports*. **5.** 345-357 (2019).
1153 https://link.springer.com/article/10.1007/s40641-019-00145-8
1154 [134.] Maher, P., Kelleher, M. E., Sansom, P. G. & Methven, J. Is the subtropical jet shifting
1155 poleward? *Climate Dynamics.* **54**, 1741-1759 (2020).
1156 https://link.springer.com/content/pdf/10.1007/s00382-019-05084-6.pdf
1157 [135.] Held, I. M. The general circulation of the atmosphere. Program in Geophysical Fluid
1158 Dynamics, Woods Hole Oceanographic Institute. 179 pp. 2000.
1159 https://darchive.mblwhoilibrary.org/handle/1912/15
1160 [136.] Davis, N. & Birner, T. On the discrepancies in tropical belt expansion between
1161 reanalyses and climate models and among tropical belt width metrics. *J. Climate.*
1162 **30** (4): 1211-1231 (2017).
1163 https://journals.ametsoc.org/view/journals/clim/30/4/jcli-d-16-0371.1.xml
1164 [137.] Menzel M. E., Waugh, D. & Grise, K. Disconnect between Hadley cell and subtropical
1165 jet variability and response to increased $CO_2$. *Geophysical Research Letters.* **46**,

7045-7053 (2019). https://agupubs.onlinelibrary.wiley.com/doi/full/10.1029/2019GL083345

[138.] Waugh, D. W. et al. Revisiting the relationship among metrics of tropical expansion. *J. Climate.* **31** (18), 7565-7581 (2018). https://journals.ametsoc.org/view/journals/clim/31/18/jcli-d-18-0108.1.xml

[139.] Chemke, R. & Polvani, L. M. Exploiting the abrupt 4 x CO2 scenario to elucidate tropical expansion mechanisms. *J. Climate*. **32** (3), 859-875 (2019). https://journals.ametsoc.org/jcli/article/32/3/859/89041/Exploiting-the-Abrupt-4-CO2-Scenario-to-Elucidate

[140.] Raghavendra, A., Roundy, P. E. & Zhou, L. Trends in tropical wave activity from the 1980s to 2016. *J. Climate*. **32** (5), 1661-1676 (2019). https://journals.ametsoc.org/jcli/article/32/5/1661/89213

[141.] Emanuel, K. The behaviour of a simple hurricane model using a convective scheme based on subcloud-later entropy equilibrium. *J. Atmos. Sci.* **52** (22): 3960-3968 (1995). https://journals.ametsoc.org/jas/article/52/22/3960/23939/The-Behavior-of-a-Simple-Hurricane-Model-Using-a

[142.] Held, I. M. & Soden, B. J. Robust responses of the hydrological cycle to global warming. *J. Climate.* **19** (21), 5686-5699 (2006). https://journals.ametsoc.org/view/journals/clim/19/21/jcli3990.1.xml

[143.] Chavas, D. R. & Reed, K. A. Dynamical Aquaplanet Experiments with Uniform Thermal Forcing: System Dynamics and Implications for Tropical Cyclone Genesis and Size. *J. Atmos. Sci*. **76**(8): 2257-2274 (2019). https://journals.ametsoc.org/jas/article/76/8/2257/343816/Dynamical-Aquaplanet-Experiments-with-Uniform

[144.] Bembenek, E., Merlis, T. M. & Straub, D. N. Influence of latitude and moisture effects on the barotropic instability of an idealised ITCZ. *J. Atmos. Sci. In press* (2021). Preprint: *https://journals.ametsoc.org/view/journals/atsc/aop/JAS-D-20-0346.1/JAS-D-20-0346.1.xml*

[145.] Ferreira, R. N. & Schubert, W. H. Barotropic aspects of ITCZ breakdown. *J. Atmos. Sci.* **54** (2), 261-285 (1997). https://journals.ametsoc.org/view/journals/atsc/54/2/1520-0469_1997_054_0261_baoib_2.0.co_2.xml

[146.] Klotzbach, P. The Madden-Julian Oscillation's impacts on worldwide tropical cyclone activity. *J. Climate*. **27** (6), 2317-2330 (2014). https://journals.ametsoc.org/jcli/article/27/6/2317/34838/The-Madden-Julian-Oscillation-s-Impacts-on

[147.] Fine, C. M., Johnson, R. H., Ciesielski, P. E. & Taft, R. K. The role of topographically induced vortices in tropical cyclone formation over the Indian Ocean. *Mon. Wea. Rev.* **144** (12), 4827-4847 (2016). https://journals.ametsoc.org/view/journals/mwre/144/12/mwr-d-16-0102.1.xml

[148.] Rios-Berrios, R., Medeiros, B. & Bryan, G. H. Mean climate and tropical rainfall variability in aquaplanet simulations using the model for prediction across scales – atmosphere. *JAMES.* **12** (10), e2020MS002102 (2020). https://agupubs.onlinelibrary.wiley.com/doi/abs/10.1029/2020MS002102

[149.] Sriver, R.L. and Huber, M. Observational evidence for an ocean heat pump induced by tropical cyclones. *Nature*, **44** *7* (7144), pp.577-580 (2007).

[150.] Korty, R.L., Emanuel, K.A. and Scott, J.R. Tropical cyclone–induced upper-ocean mixing and climate: Application to equable climates. *Journal of Climate*, *21*(4),

pp.638-654 (2008). https://journals.ametsoc.org/view/journals/clim/21/4/2007jcli1659.1.xml

[151.] Huang, A., Li, H., Sriver, R.L., Fedorov, A.V. and Brierley, C.M. Regional variations in the ocean response to tropical cyclones: Ocean mixing versus low cloud suppression. *Geophysical Research Letters*, *44*(4), pp.1947-1955 (2017).

[152.] O'Neill, B. C. et al. The Scenario Model Intercomparison Project (ScenarioMIP) for CMIP6. *Geosci. Model Dev.* **9**, 3461-3482 (2016). https://gmd.copernicus.org/articles/9/3461/2016/gmd-9-3461-2016.pdf

[153.] NASA's Earth Observing System Data and Information System (EOSDIS). Fields from the Visible Infrared Imaging Radiometer Suite (VIRRS) aboard the Suomi National Polar-orbiting Partnership (NPP) satellite. Weblink: https://worldview.earthdata.nasa.gov/. Accessed on 21st September 2021.

[154.] Bony, S. et al. Cloud, circulation, and climate sensitivity. *Nature Geoscience.* **8**, 261-268. (2015). https://www.nature.com/articles/ngeo2398

[155.] Copernicus Climate Change Service (C3S). ERA5: Fifth generation of ECMWF atmospheric reanalyses of the global climate . Copernicus Climate Change Service Climate Data Store (CDS) (2017). [Accessed on 21st August 2020]. https://cds.climate.copernicus.eu/cdsapp#!/home

[156.] Knapp, K. R., Diamond, H. J., Kossin, J. P., Kruk, M. C. & Schreck, C. J. International Best Track Archive for Climate Stewardship (IBTrACS) Project, Version 4. [v04r00]. NOAA National Centers for Environmental Information (2018). https://www.ncdc.noaa.gov/ibtracs/index.php?name=ib-v4-access. [May 21st 2021].

[157.] Dix, M. et al. CSIRO-ARCCSS ACCESS-CM2 model output prepared for CMIP6 CMIP. Earth System Grid Federation (2019). doi: https://doi.org/10.22033/ESGF/CMIP6.4271

[158.] Ziehn, T. et al. CSIRO ACCESS-ESM1.5 model output prepared for CMIP6 C4MIP. Earth System Grid Federation. (2019). doi: https://doi.org/10.22033/ESGF/CMIP6.2286

[159.] Zhang, F. et al. BCC BCC-CSM2MR model output prepared for CMIP6 C4MIP. Earth System Grid Federation. (2019). doi: https://doi.org/10.22033/ESGF/CMIP6.1723

[160.] Rong, X. CAMS CAMS_CSM1.0 model output prepared for CMIP6 CMIP. Earth System Grid Federation (2019). doi: https://doi.org/10.22033/ESGF/CMIP6.1399

[161.] Danabasoglu, G. NCAR CESM2-WACCM model output prepared for CMIP6 AerChemMIP. Earth System Grid Federation. (2019). doi: https://doi.org/10.22033/ESGF/CMIP6.10023

[162.] Huang, W. THU CIESM model output prepared for CMIP6 CMIP. Earth System Grid Federation. (2019). doi: https://doi.org/10.22033/ESGF/CMIP6.1352

[163.] Swart, N. C. et al. CCCma CanESM5 model output prepared for CMIP6 C4MIP. Earth System Grid Federation. (2019). doi: https://doi.org/10.22033/ESGF/CMIP6.1301

[164.] EC-Earth Consortium (EC-Earth). EC-Earth-Consortium EC-Earth3-Veg model output prepared for CMIP6 CMIP. Earth System Grid Federation. (2019). doi: https://doi.org/10.22033/ESGF/CMIP6.642

[165.] Silvers, L. et al. NOAA-GFDL GFDL-CM4 model output prepared for CMIP6 CFMIP. Earth System Grid Federation. (2018). doi: https://doi.org/10.22033/ESGF/CMIP6.1641

[166.] Horowitz, L. W. et al. NOAA-GFDL GFDL-ESM4 model output prepared for CMIP6 AerChemMIP. Earth System Grid Federation. (2018). doi: https://doi.org/10.22033/ESGF/CMIP6.1404

[167.] Volodin, E. et al. INM INM-CM4-8 model output prepared for CMIP6 CMIP. Earth System Grid Federation. (2019). doi: https://doi.org/10.22033/ESGF/CMIP6.1422

[168.] Volodin, E. et al. INM INM-CM5-0 model output prepared for CMIP6 CMIP. Earth System Grid Federation. (2019). doi: https://doi.org/10.22033/ESGF/CMIP6.1423

[169.] Boucher, O. et al. IPSL IPSL-CM6A-LR model output prepared for CMIP6 C4MIP. Earth System Grid Federation. (2018). doi: https://doi.org/10.22033/ESGF/CMIP6.1521

[170.] Takemura, T. MIROC MIROC6 model output prepared for CMIP6 AerChemMIP. Earth System Grid Federation. (2019). doi: https://doi.org/10.22033/ESGF/CMIP6.9121

[171.] Jungclaus, J. et al. MPI-M MPIESM1.2-HR model output prepared for CMIP6 CMIP. Earth System Grid Federation. (2019). doi: https://doi.org/10.22033/ESGF/CMIP6.741

[172.] Yukimoto, S. et al. MRI MRI-ESM2.0 model output prepared for CMIP6 AerChemMIP. Earth System Grid Federation. (2019). doi: https://doi.org/10.22033/ESGF/CMIP6.633

[173.] Seland, Ø. et al. NCC NorESM2-LM model output prepared for CMIP6 CMIP. Earth System Grid Federation. (2019). doi: https://doi.org/10.22033/ESGF/CMIP6.502

[174.] Emanuel, K. An air-sea interaction theory for tropical cyclone. Part I: Steady state maintenance. *J. Atmos. Sci.* **43**, 585-605 (1986).

https://journals.ametsoc.org/jas/article/43/6/585/21614/An-Air-Sea-Interaction-Theory-for-Tropical

[175.] Emanuel, K. The dependence of hurricane intensity on climate. *Nature*. **326**, 483-485 (1987). https://www.nature.com/articles/326483a0.

[176.] Kossin, J. P., Knapp, K. R., Olander, T. L. & Velden, C. S. Global increase in major tropical cyclone exceedance probability over the past four decades. *PNAS.* **117(**22). 11975-11980 (2020). https://www.pnas.org/content/117/22/11975

[177.] Reyes, A. R. and Yang, D. Spontaneous cyclogenesis without radiative and surface flux feedbacks. *J. Atmos. Sci.* **EOR**. (2021). https://journals.ametsoc.org/view/journals/atsc/aop/JAS-D-21-0098.1/JAS-D-21-0098.1.xml

[178.] Tang, B. & Emanuel, K. A Ventilation Index for Tropical Cyclones. *BAMS*. **12.** 1901-1912 (2012). https://journals.ametsoc.org/bams/article/93/12/1901/60272/A-Ventilation-Index-for-Tropical-Cyclones

[179.] Holland, G. J. Tropical cyclone motion: environmental interaction plus a beta effect. *J. Atmos. Sci.* **40** (2). 328-342 (1983). https://journals.ametsoc.org/jas/article/40/2/328/20554/Tropical-Cyclone-Motion-Environmental-Interaction

[180.] Smith, R. B. A hurricane beta-drift law. *J. Atmos. Sci.* **50** (18), 3213-3215 (1993). https://journals.ametsoc.org/view/journals/atsc/50/18/1520-0469_1993_050_3213_ahbdl_2_0_co_2.xml

[181.] Arakawa, A. & Schubert, W. H. Interaction of a cumulus cloud ensemble with the large-scale environment. Part I. *J. Atmos. Sci.* **31** (3). 674-701 (1974). https://journals.ametsoc.org/jas/article/31/3/674/18668/Interaction-of-a-Cumulus-Cloud-Ensemble-with-the

[182.] Sobel, A. H. & Bretherton, C. S. Modeling tropical precipitation in a single column. *J. Climate*. **13,** 4378-4392 (2000). https://journals.ametsoc.org/jcli/article/13/24/4378/29455/Modeling-Tropical-Precipitation-in-a-Single-Column

[183.] Emanuel, K. Inferences from simple models of slow, convective coupled processes. *J. Atmos. Sci.* **76** (1): 195-208 (2019). https://journals.ametsoc.org/jas/article/76/1/195/107328

[184.] Back, L. E. & Bretherton, C. S. On the relationship between SST gradients, boundary layer winds, and convergence over the tropical oceans. *J. Climate.* **22** (15): 4182-4196 (2009). https://journals.ametsoc.org/jcli/article/22/15/4182/32181

**Correspondence and requests for materials** should be addressed to JS (joshua.studholme@yale.edu).

**Acknowledgements** We thank the four anonymous reviewers and the editor for their constructive comments that have improved the manuscript. We also thank Mike Byrne (at the Universities of St. Andrews & Oxford) and Gabriel Vecchi (at Princeton University) for helpful discussions. We thank Colin Zarzycki (at Penn State University) for providing the PETM data and Naomi Henderson (at Columbia University) for assistance with CMIP6 data access. We recognise and thank NASA, NOAA, ECMWF, and the CMIP6 group of the World Climate Research Programme for making their data publicly and freely available. JS and AF have been supported in part by grants from NASA (NNX17AH21G), NOAA (NA20OAR4310377) and the ARCHANGE project of the "Make our planet great again" program (ANR-18-MPGA-0001, the Government of the French Republic). SG benefited from the Russian Science Foundation grant #20-17-00139 and from the Agreement

#14.W0331.0006 with the Russian Ministry of Science and Higher Education. KE is supported by the U.S.'s National Science Foundation (ICER-1854929). KH acknowledges funding from the U.K.'s Natural Environment Research Council.

**Author contributions** JS conceived the study, wrote the drafts, produced the figures, and led the preparation of the manuscript with input from all the co-authors.

**Competing interests** The authors declare no competing interests.

**Data Availability Statement** All data used in this study is freely and publicly available in perpetuity.

*Tropical cyclone observational record* The tropical cyclone data for the contemporary period (Fig. 2 and Ext. Data Fig. 4) is plotted directly from the International Best Track Archive for Climate Stewardship[156.] (IBTrACS). These data are freely available at https://doi.org/10.25921/82ty-9e16. Version v04r00 was downloaded and the World Meteorological Organisation's homogenisation was used.

*Contemporary environment* Fields, used in Figs. 2 and 4, and Extended Data Figs. 4, 6 and 8, were taken from the European Centre for Medium Range Weather Forecasting's (ECMWF's) ERA5 reanalysis product[155.]. All data was downloaded at native horizonal resolution (¼ x ¼ degree) as monthly means for the years 1979 to 2020. These raw data are freely and publicly available for download at https://doi.org/10.24381/cds.6860a573.

*Cloud-resolving modelling* The idealised cloud-resolving modelling data is replotted from ref.[32.]. This data is freely available in the following Dryad repository: doi:10.5061/dryad.8pk0p2np2

*Paleocene-Eocene Thermal Maximum modelling data* These data, from ref. [34.], are available at https://doi.org/10.1016/j.palaeo.2021.110421.

*CMIP6* Data for the ITCZ plotted in Fig. 6 and Ext. Data Fig. 7 was taken from 17 model centres that contributed to Climate Model Intercomparison Project Phase 6 (CMIP6). These data are available from the Earth System Grid Federation. Our CMIP6 analysis relies on subsets of the total model ensemble (+50 models). We used data from the following models: ACCESS-CM2[157.], ACCESS-ESM1-5[158.], BCC-CSM2-MR[159.], CAMS-CSM1-0[160.], CESM2-WACCM[161.], CIESM[162.], CanESM5[163.], EC-Earth3-Veg[164.], GFDL-CM4[165.], GFDL-ESM4[166.], INM-CM4-8 [167.], INM-CM5-0[168.], IPSL-CM6A-LR [169.], MIROC6[170.], MPI-ESM1-2-HR[171.], MRI-ESM2-0[172.], NorESM2-LM[173.].

**METHODS**

*a. Tropical cyclone track density*

Track density is computed from the IBTrACS archive as the annual count of TC track points within 4 degrees of each grid square (using a ¼ by ¼ degree grid to match the ECMWF environmental fields). The temporal resolution of the underlying track data is 3-hourly. Note that North Indian Ocean tracks are masked since TCs there began to be recorded in the dataset only in recent years.

*b. Climate diagnostics*

Climate diagnostics shown in Figs. 4, 6 and Extended Data Fig. 7 are computed from ERA5 data (detailed in Section S1.b directly above) using the following methods:

*Tropical cyclone potential intensity* – Potential intensity (PI, units $ms^{-1}$) calculations were done for ERA5 data using Daniel Gilford's pyPI algorithm[185.], an implementation of the Bister and Emanuel algorithm[186.]. This method is based on the following expression:

$$PI^2 = \frac{C_k}{C_D} \times \frac{T_s}{T_o} \times (CAPE^* - CAPE)|_{RMW}, \quad [\text{M1.}]$$

where $C_k$ and $C_D$ are the exchange coefficients for enthalpy and momentum, $T_s$ and $T_o$ are temperature at the sea surface and at the TC outflow branch in the upper troposphere, both in units of K. $CAPE^*$ and $CAPE$ are the convective available potential energies of the saturated air lifted from the ocean surface to the outflow level and of boundary layer air respectively, both evaluated at the radius of maximum winds (RMW). An alternative, more conceptually intuitive, expression for PI can be also used[187.]:

$$PI^2 = \underbrace{\frac{C_k}{C_D}}_{Exchange\ coefficients} \times \underbrace{\frac{(T_s - T_o)}{T_o}}_{Modified\ Carnot\ efficiency} \times \underbrace{(k_s^* - k)}_{\substack{Air-sea\ thermodynamic \\ disequilibrium}}, \quad [\text{M2.}]$$

where $k_s^*$ is the saturation moist enthalpy of air right at the sea surface and $k$ is the moist enthalpy of air in the boundary layer overlying the surface. Expression M1 is more accurate than M2 because the former better estimates the amount of energy available for convection[188.]. PI can be then decomposed into the terms in M2 while using expression M1 to compute thermodynamic disequilibrium as a residual.

*Genesis potential* – The genesis potential (GP) is calculated using the form[189.]:

$$GP = |\eta|^3 \chi^{-\frac{4}{3}} \text{MAX}[PI - 35\text{ms}^{-1}), 0]^2 (V_{shear} + 25ms^{-1})^{-4},$$

where $\eta$ is absolute vorticity of the flow at 850 hPa, capped at the value of 5 x $10^{-5}s^{-1}$, PI is expressed as a flow speed, $V_{shear}$ is the magnitude of wind shear estimated as wind speed difference between 850 and 250 hPa (in m/s). $\chi$ is the moist entropy deficit in the middle troposphere defined as

$$\chi = \frac{s_b - s_m}{s_s^* - s_b}$$

where $s_b$, $s_m$ and $s_s^*$ are the moist entropies of the boundary layer and middle troposphere, and the saturation moist entropy at the sea surface, respectively. Moist entropy *s* is defined as

$$s = c_p lnT - R_d lnp + \frac{L_v q_v}{T} - R_v q lnH,$$

where *T* and *p* are temperature (in K) and pressure, $c_p$is the specific heat capacity at constant pressure of air, $L_v$ is the latent heat of vaporisation, $q$ is the specific humidity, $R_d$ and $R_v$ are the gas constants for dry air and water vapour respectively, and *H* is the relative humidity.

*Moist Static Energy* is defined here as follows:

$$h = c_p T + gz + L_v q_v,$$

where *g* is gravitational acceleration, *z* is the height above the surface.

*ITCZ metrics* - Three metrics for the Intertropical Convergence Zone (ITCZ) were computed using CMIP6 data, all by standard methods (e.g. ref.[131.]), *intensity, latitude and width* as described below. All metrics are computed from hemispheric zonal-mean precipitation [units mm $day^{-1}$] and are averaged over the last three decades of each CMIP6 experiment during TC seasons for the respective hemisphere – July to October in the northern hemisphere and January to March in the southern hemisphere. These metrics are plotted in Fig. 6 and

Extended Data Fig. 7. against the global maximum in zonal-mean sea surface temperature (SST, units ºC) during the respective TC season.

*ITCZ intensity* - is defined as the maximum in zonal-mean seasonal-mean precipitation.

*ITCZ latitude* - is defined as the latitude of the maximum in zonal-mean seasonal-mean precipitation.

*ITCZ width* - is defined as the cartesian distance between latitudes of zonal-mean seasonal-mean precipitation crossing the 5 mm $day^{-1}$ threshold on either side of the ITCZ latitude.

**METHODS REFERENCES**


[185.] Gilford, D. M. pyPI (v1.3): Tropical Cyclone Potential Intensity Calculations in Python. Geosci. Model Dev. **14**. 2351-2369 (2021). https://gmd.copernicus.org/articles/14/2351/2021/gmd-14-2351-2021.pdf

[186.] Bister, M. & Emanuel, K. A. Low frequency variability of tropical cyclone potential intensity. 1. Interannual and interdecadal variability. *J. Geophys. Research : Atmospheres.* **107** (D24). 4801 (2002). https://agupubs.onlinelibrary.wiley.com/doi/full/10.1029/2001JD000776

[187.] Emanuel, K. Tropical cyclones. *Ann. Rev. of Earth and Planetary Sciences.* **31** 75-104 (2003). https://www.annualreviews.org/doi/10.1146/annurev.earth.31.100901.141259

[188.] Garner, S. The relationship between hurricane potential intensity and CAPE. *J. Atmos. Sci.* **72**, 141-163. (2015). https://journals.ametsoc.org/view/journals/atsc/72/1/jas-d-14-0008.1.xml

[189.] Emanuel, K. Tropical cyclone activity downscaled from NOAA-CIRES reanalysis, 1908-1958. *JAMES.* **2** (1) (2010). https://agupubs.onlinelibrary.wiley.com/doi/full/10.3894/JAMES.2010.2.1

## EXTENDED DATA

## [EXTENDED DATA FIGURE 1]

**Extended Data Fig. 1 | The development and intensification of Hurricane Goni (2020, peak intensity 195 mph).** Poorly organised convection over the west Pacific warm pool aggregates over the course of three days between October 22$^{th}$ and 24$^{th}$ (**a b c**), and then acquires coherent rotation over the subsequent three days (25$^{th}$ to 27$^{th}$, **d e f**) while propagating westward away from its seeding region. Between Oct 28$^{th}$ and 30$^{th}$, Goni developed into a fully-fledged TC (**g h i**) and made the strongest recorded landfall event by landfalling in the Philippines on Oct 31$^{st}$**.** Data from ref [153.].

**[EXTENDED DATA FIGURE 2]**

**Extended Data Fig. 2 | The extratropical transition of Hurricane Paulette and the simultaneous tropical transition of Subtropical Storm Alpha.** Hurricane Paulette, which originally developed out of an easterly wave on Sept 7th, reached its peak intensity on Sept 14th (105 mph) and then underwent extratropical transition to become an extratropical cyclone on Sept 17th. It then moved south and underwent tropical transition to intensify as a tropical cyclone on Sept 22. Subtropical Storm Alpha (peak intensity 50 mph) was the first ever tropical cyclone to make landfall in Portugal and the eastern-most genesis event in the North Atlantic record. At the same time as these events, a rare medicane tropical cyclogenesis event occurred forming Cyclone Ianos (peak intensity 75 mph) which made landfall in Greece, seen in Extended Data Figure 3. Data from ref. [153.].

**[EXTENDED DATA FIGURE 3]**

**Extended Data Fig. 3 | The North Atlantic on September 16th, 2020.** Hurricane Sally (peak intensity 105 mph) can be seen making landfall over Alabama in the US, while Hurricane Teddy (peak intensity 140 mph) was intensifying over the tropical North Atlantic and to its northeast, Tropical Storm Vicky is being weakened by strong environmental wind shear. Hurricane Paulette can be seen midway through its extratropical transition of the coast of Nova Scotia and the extratropical cutoff low that became Subtropical Storm Alpha can be seen off the coast of Portugal. In the Mediterranean, the rare Medicane Ianos can be seen south of Italy. Tropical Storms Wilfred and Beta later developed out of the organising convection visible off equatorial Africa and in the Gulf of Mexico respectively. Data from ref. [153.].

**[EXTENDED DATA FIGURE 4]**

**Extended Data Fig. 4 | Planetary-scale atmospheric circulation, precipitation, and TC activity during the simulated Paleocene-Eocene Thermal Maximum (PETM) and the modern period.** **a, c** First tracked positions and **b, d** TC tracks for PETM and modern climates. The green overlay in **b** and **d** show the 6.5 mm/day climatological TC season precipitation contours. PETM data is replotted from simulations in ref. [34.] and modern data is from IBTrACs (methods). Red and blue dots are as in Fig. 2, blue for 1980-1999 and red for 2000-2019. Note that the lysis definition marking the end of the tracks between the PETM tracking and modern data are not easily reconcilable. The suppression of the low latitude TCs in the PETM is related to the splitting of the summertime subtropical and eddy-driven jets (Extended Data Fig. 5 and Fig. 5).

**[EXTENDED DATA FIGURE 5]**

**Extended Data Fig. 5 | Zonal-mean large-scale climate and north-south TC lifetime maximum intensity during the Paleocene-Eocene Thermal Maximum (PETM, $CO_2$ 1590 ppm).** Replotted from the ~0.25-degree resolution atmospheric GCM simulations of ref. [34.]. Note the strong agreement on coincident jet split and TC activity in the midlatitude with the idealised cloud-system-resolving aquaplanet simulations of ref. [32.] shown in Fig. 5 of the main manuscript.

**[EXTENDED DATA FIGURE 6]**

**Extended Data Fig. 6 | Surface precipitation and tropospheric winds and recent linear trends from ERA5.** **a**, **b**, **c** the 1980-2019 precipitation, and upper (300 hPa) and lower level (850 hPa) wind climatology for the tropical cyclone season (July through September for the northern hemisphere, January through March for the southern hemisphere). **b** The linear trend for the same seasons over the same period. Only trends for which *p* values are < 0.05 are plotted. The contour lines in **b**, **d**, and **f** are used to visualise the ITCZ (6.5 mm $day^{-1}$), and the jet streams (5 m $s^{-1}$ in the lower troposphere in **d** and 20 m $s^{-1}$ in the upper troposphere in **f**). Data from ERA5[155.].

**[EXTENDED DATA FIGURE 7]**

**Extended Data Fig. 7 | As in Fig. 6 but for the southern hemisphere during TC season there: January-February-March.** Note the wide range in projections for the atmosphere only ('amip') simulations in blue, highlighting the significance of atmosphere-ocean coupling for tropical climate. The largest contribution to this "southern ITCZ" comes from the South Pacific Convergence Zone (SPCZ). Also note that these results may be affected by the models' double-ITCZ problem, which exaggerates the magnitude of the tropical convection to the south of the equator. Data from refs [157.] [158.] [159.] [160.] [161.] [162.] [163.] [164.] [165.] [166.] [167.] [168.] [169.] [170.] [171.] [172.] [173.].

**[EXTENDED DATA FIGURE 8]**

**Extended Data Fig. 8 | Surface enthalpy fluxes and recent linear trends from ERA5 (1980-2019).** Plotted as in Extended Data Fig. 6. Climatology and trends are for the tropical cyclone season (July through September for the northern hemisphere, January through March for the southern hemisphere). Data from ERA5[155.].

---

**ENDS**

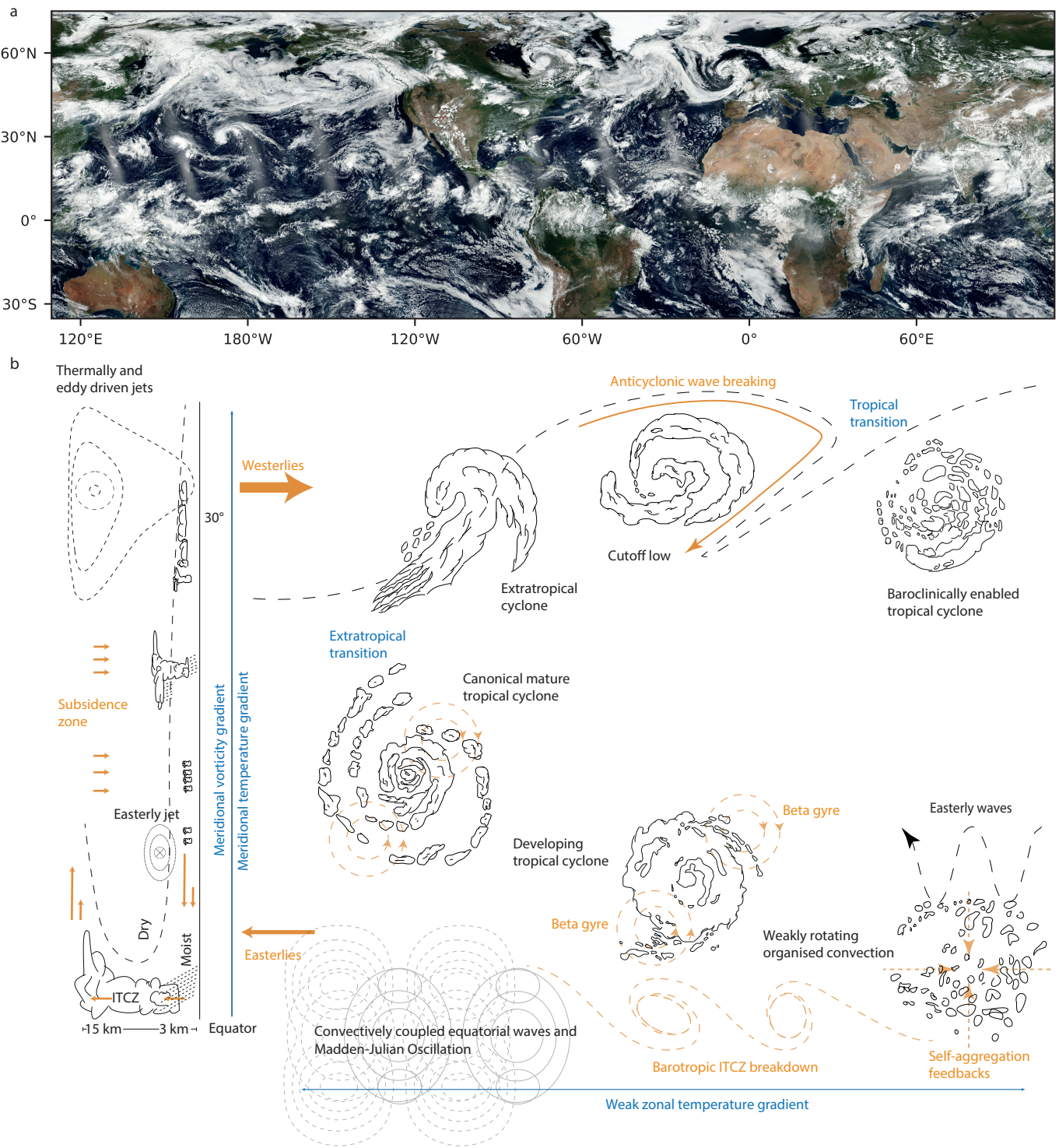
a
60°N
30°N
0°
30°S
120°E
180°W
120°W
60°W
0°
60°E
b
Thermally and eddy driven jets
30°
Westerlies
Subsidence zone
Easterly jet
Dry
Moist
ITCZ
15 km
3 km
Equator
Meridional vorticity gradient
Meridional temperature gradient
Easterlies
Anticyclonic wave breaking
Tropical transition
Cutoff low
Extratropical cyclone
Baroclinically enabled tropical cyclone
Extratropical transition
Canonical mature tropical cyclone
Developing tropical cyclone
Beta gyre
Beta gyre
Easterly waves
Weakly rotating organised convection
Convectively coupled equatorial waves and Madden-Julian Oscillation
Barotropic ITCZ breakdown
Self-aggregation feedbacks
Weak zonal temperature gradient

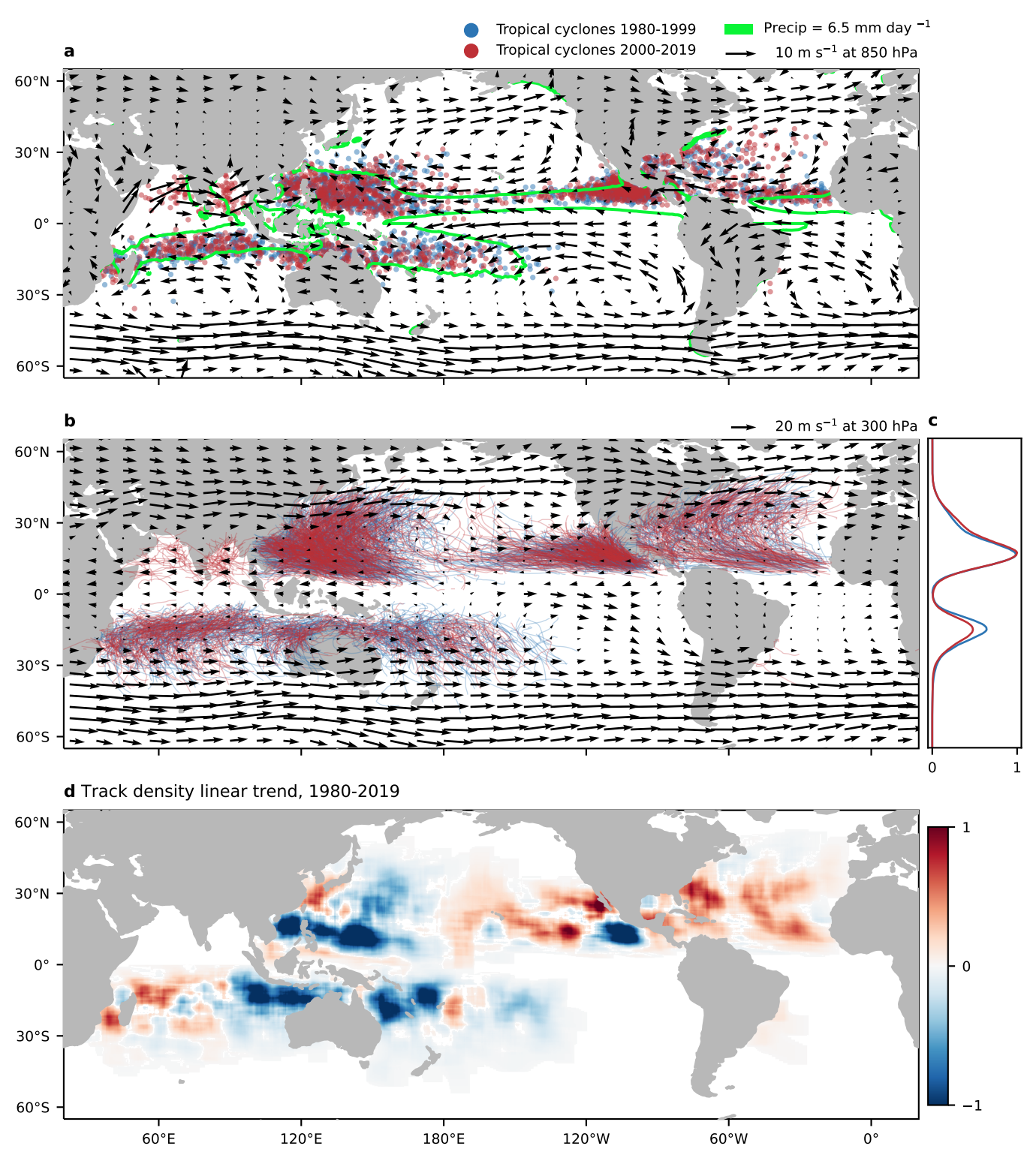
Tropical cyclones 1980-1999
Tropical cyclones 2000-2019
Precip = 6.5 mm day $^{-1}$
10 m s$^{-1}$ at 850 hPa
a
60°N
30°N
0°
30°S
60°S
b
20 m s$^{-1}$ at 300 hPa
c
0
1
d Track density linear trend, 1980-2019
60°E
120°E
180°E
120°W
60°W
0°
1
0
−1

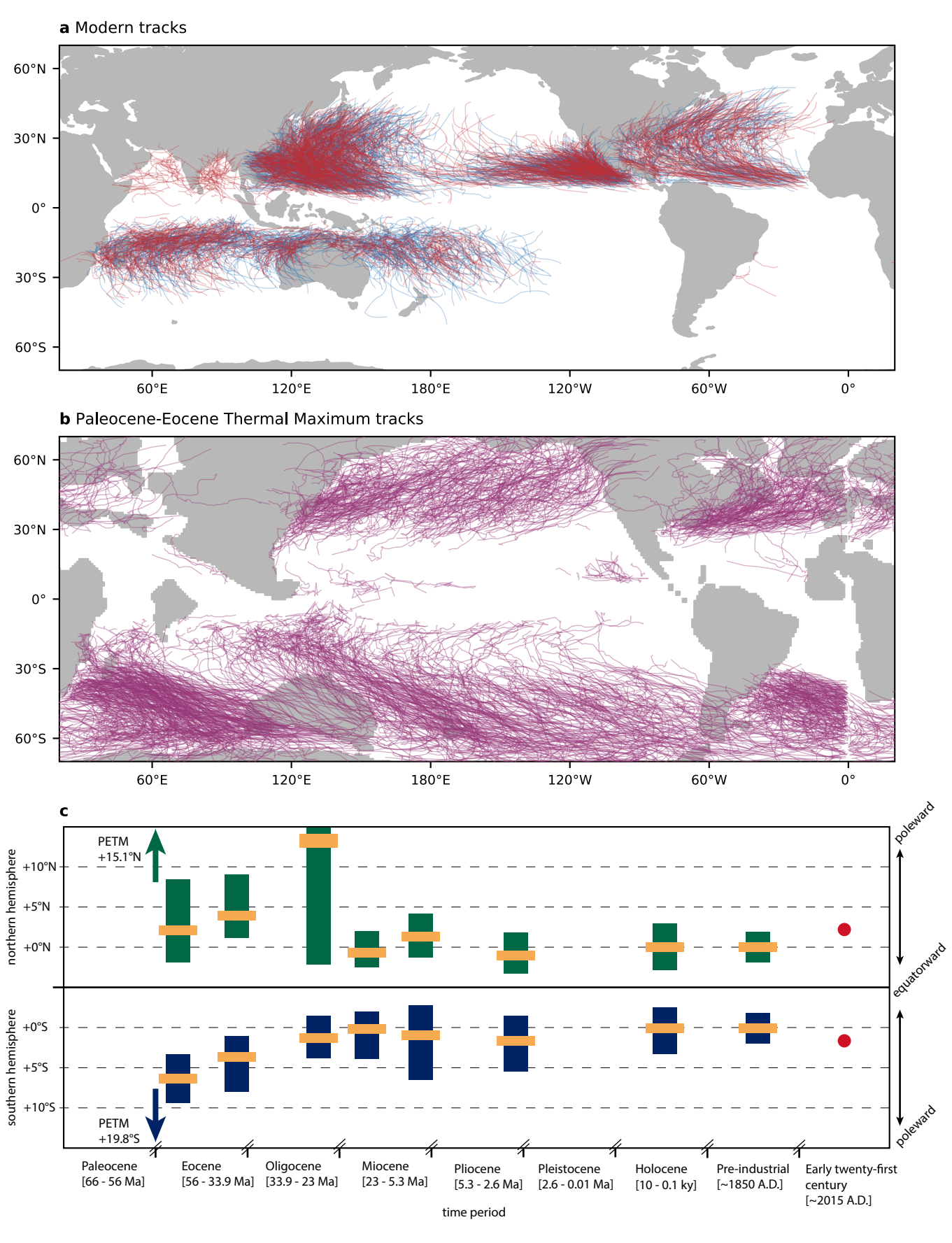
a Modern tracks
60°N
30°N
0°
30°S
60°S
60°E
120°E
180°E
120°W
60°W
0°
b Paleocene-Eocene Thermal Maximum tracks
60°N
30°N
0°
30°S
60°S
60°E
120°E
180°E
120°W
60°W
0°
c
northern hemisphere
+10°N
+5°N
+0°N
PETM
+15.1°N
southern hemisphere
+0°S
+5°S
+10°S
PETM
+19.8°S
poleward
equatorward
poleward
Paleocene
[66 - 56 Ma]
Eocene
[56 - 33.9 Ma]
Oligocene
[33.9 - 23 Ma]
Miocene
[23 - 5.3 Ma]
Pliocene
[5.3 - 2.6 Ma]
Pleistocene
[2.6 - 0.01 Ma]
Holocene
[10 - 0.1 ky]
Pre-industrial
[~1850 A.D.]
Early twenty-first century
[~2015 A.D.]
time period

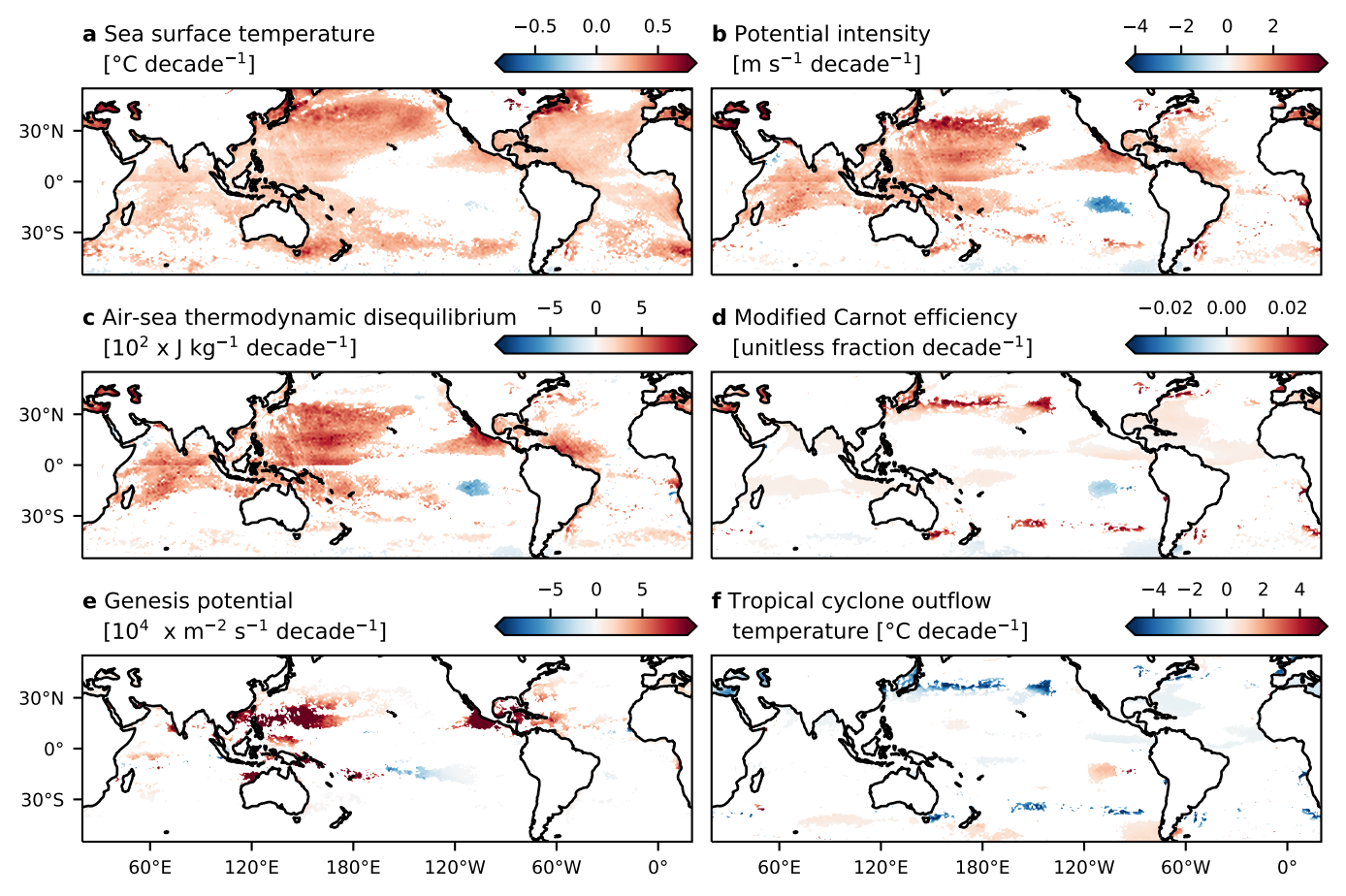
a Sea surface temperature
[°C decade−1]
−0.5 0.0 0.5
b Potential intensity
[m s−1 decade−1]
−4 −2 0 2
c Air-sea thermodynamic disequilibrium
[10² x J kg−1 decade−1]
−5 0 5
d Modified Carnot efficiency
[unitless fraction decade−1]
−0.02 0.00 0.02
e Genesis potential
[10⁴ x m−2 s−1 decade−1]
−5 0 5
f Tropical cyclone outflow
temperature [°C decade−1]
−4 −2 0 2 4
30°N
0°
30°S
60°E 120°E 180°E 120°W 60°W 0°

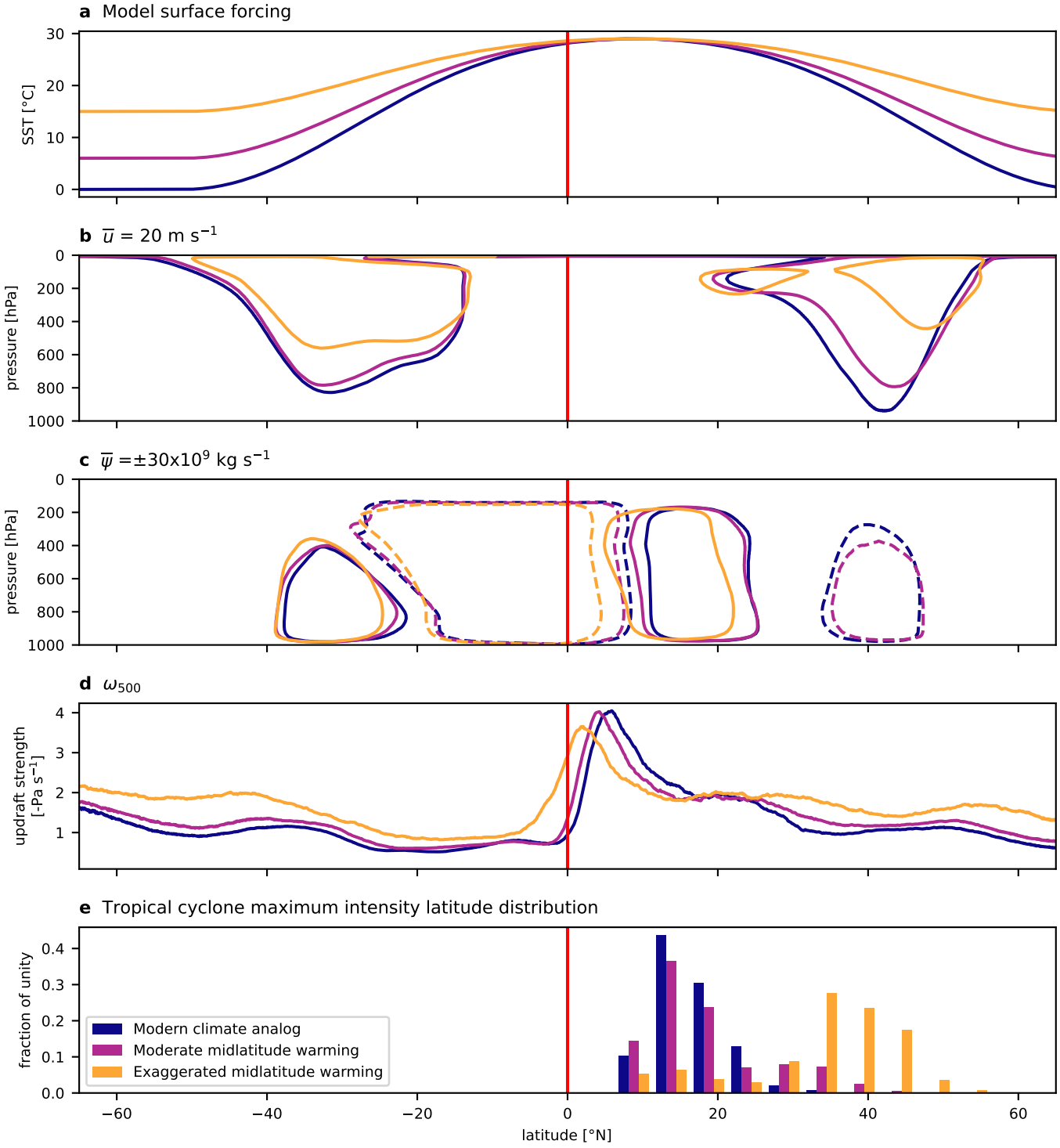
a Model surface forcing
SST [°C]
b $\overline{u}$ = 20 m s$^{-1}$
pressure [hPa]
c $\overline{\psi}$ =±30x10$^9$ kg s$^{-1}$
pressure [hPa]
d $\omega_{500}$
updraft strength [-Pa s$^{-1}$]
e Tropical cyclone maximum intensity latitude distribution
fraction of unity
Modern climate analog
Moderate midlatitude warming
Exaggerated midlatitude warming
latitude [°N]

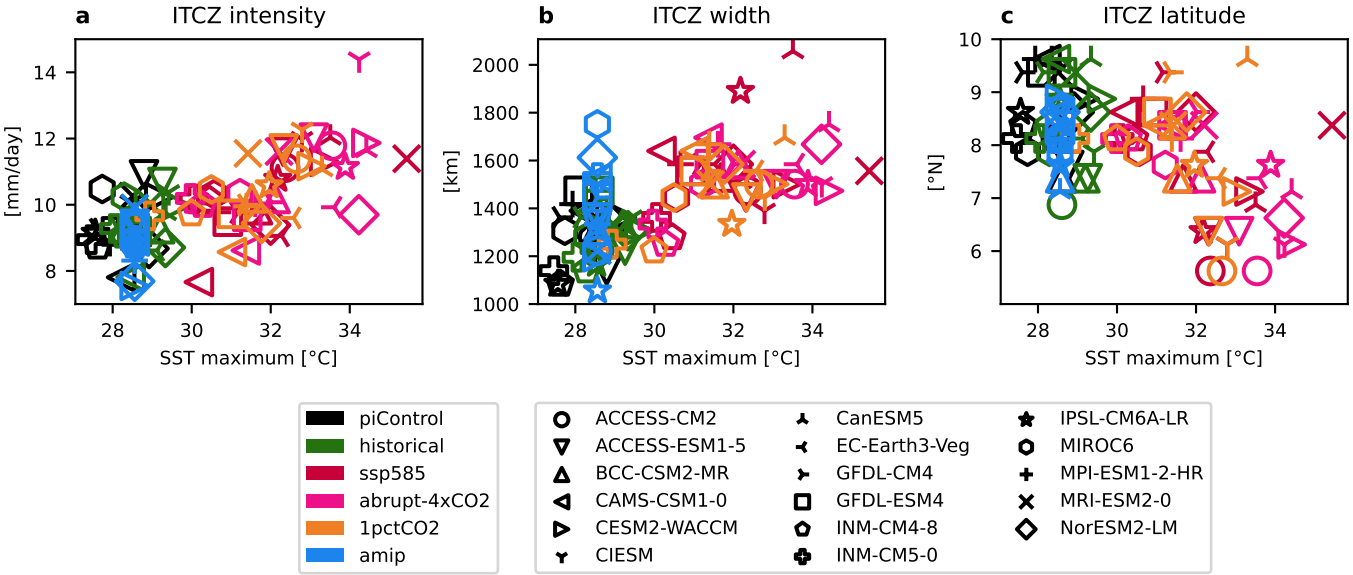
a
ITCZ intensity
[mm/day]
SST maximum [°C]
b
ITCZ width
[km]
SST maximum [°C]
c
ITCZ latitude
[°N]
SST maximum [°C]
piControl
historical
ssp585
abrupt-4xCO2
1pctCO2
amip
ACCESS-CM2
ACCESS-ESM1-5
BCC-CSM2-MR
CAMS-CSM1-0
CESM2-WACCM
CIESM
CanESM5
EC-Earth3-Veg
GFDL-CM4
GFDL-ESM4
INM-CM4-8
INM-CM5-0
IPSL-CM6A-LR
MIROC6
MPI-ESM1-2-HR
MRI-ESM2-0
NorESM2-LM